Journal of Archaeological Science 54 (2015) 193–209

Contents lists available at ScienceDirect

Journal of Archaeological Science

journal homepage: http://www.elsevier.com/locate/jas

Anthropogenic origin of siliceous scoria droplets from Pleistocene and Holocene archaeological sites in northern Syria

P. Thy [a, *], G. Willcox [b], G.H. Barfod [c], D.Q. Fuller [d]

[a] Department of Earth and Planetary Sciences, University of California, One Shields Avenue, Davis CA 95616, USA
[b] Archéorient CNRS, UMR 5133, Université de Lyon II Antenne d'Archéorient, Jalès, Berrias, F-07460 St-Paul-le-Jeune, France
[c] Department of Geoscience, Aarhus University, Høegh-Guldbergs Gade 2, DK-8000 Aarhus C, Denmark
[d] University College London, Institute of Archaeology, 31-34 Gordon Square, London WC1H OPY, UK

ARTICLE INFO

Article history:
Received 30 July 2014
Received in revised form
4 November 2014
Accepted 22 November 2014
Available online 16 December 2014

Keywords:
Scoria droplets
Younger Dryas impact
Settlement fires
Moderate melting temperature

ABSTRACT

Siliceous scoria droplets, measuring from 1 to 10 mm, from one late Pleistocene and four early Holocene archaeological sites in northern Syria are compared to similar droplets previously suggested to be the result of a cosmic impact at the onset of the Younger Dryas global cooling event. The findings demonstrate that the presence of siliceous scoria droplets are independent of age and thus are not specific to the beginning of the Younger Dryas. Occurrences have not been reported from natural deposits, but are instead associated with buildings destroyed by fire and thus appear to be restricted to archaeological sites. We therefore conclude that melting of building earth in ancient settlements can occur during fires reaching modest temperatures. There is no evidence to suggest that siliceous scoria droplets result from very high temperature melting of soil and are the result of a cosmic event.

1. Introduction

Siliceous scoria droplets can sometimes be obtained from sediments at archaeological sites. In the present paper we report evidence that these can form unintentionally under conditions of anthropogenic fire even in societies without the technology of ceramics or other pyrotechnical industries. This study has been prompted by the claims that scoria found on archaeological sites were formed by temperatures exceeding 2200 °C by Bunch et al. (2012) and Wittke et al. (2013). Such high temperatures, the authors suggest could only have been produced by a cosmic impact that they date to around 12,900 years ago at the beginning of the Younger Dryas interglacial cooling event. Wittke et al. (2013) suggested that an area of 50 million square kilometers, including North America, Europe, and the Middle East, was affected by the cosmic impact producing ten million tons of scoria spherules by the melting of soil and sediments. For the Old World, they only reported siliceous scoria droplets from the archaeological Middle Eastern site of Abu Hureyra in Syria. They also reported on siliceous scoria from two sites in North America (Melrose and Blackville). We report on analyses of scoria from other periods at Abu Hureyra and from four other sites in northern Syria dating between 11,300 and 10,500 years ago. We also examine a sample of vitrified earth from buildings destroyed by fire from one of the sites. Our results demonstrate that scoria occurs over a wide range of ages and that they are associated with and likely formed by human induced fire.

Vitrification or melting of siliceous materials on Old World archaeological sites prior to or unconnected with metal and ceramic manufacture has been reported from many sites. There are five main categories.

1) Partial melting is well known from the vitrified forts of Scotland and Scandinavia and is particularly well documented at Neolithic forts in Scotland. They have become known as the vitrified forts and have been the subject of numerous articles (e.g. Brothwell et al., 1974; Youngblood et al., 1978). Gordon Childe carried out experiments recreating as closely as possible the original conditions of the burned walls. He reported that the core of the heated rubble became red hot, probably reaching 800–1200 °C (Childe and Thorneycroft, 1937). Closer examination showed partial melting of the lower part of the rubble with rock particles and casts of timber preserved. The experiment proved that timber-laced walls could melt during building fire.

* Corresponding author.
E-mail addresses: pthy@ucdavis.edu (P. Thy), willcox.george@neuf.fr (G. Willcox), grybarfod@geo.au.dk (G.H. Barfod), d.fuller@ucl.ac.uk (D.Q. Fuller).

http://dx.doi.org/10.1016/j.jas.2014.11.027
0305-4403/

Friend et al. (2007, 2008) further demonstrated that partial melting in fort walls was initiated by the degradation of mica at temperatures of about 850 °C. Similar finds come from Scandinavia (Kresten and Ambrosiani, 1992). Furthermore, vitrified basalt has been found at two Bronze Age archaeological sites, Umbashi in southern Syria (Braemer et al., 2004) and Tilmen Höyük in southeast Turkey (Marocchi et al., 2010).

2) Vitrified dung has been reported from southern Africa and India, associated with sites of cattle penning. Zeuner (1959) first demonstrated experimentally that the phytoliths (ash particles) in burned dung could melt and become slag-like, and that in intervening ashy layers in South Indian mounds grass phytoliths were numerous. It has been suggested that burning was intentional and that high potassium content may have lowered the melting point of dung or plant ash causing the occasional formation of siliceous slag in ash-rich deposits. Results of chemical analyses suggest that intentional burning of dung may also partially have melted the surrounding sediment (Thy et al., 1995; Korisettar et al., 2001; Jacobson et al., 2003; Johansen, 2004; Denbow et al., 2008; Venkatasubbaiah, 2012).
3) Vitrified building earth has been observed at many Neolithic sites in southeast Europe and in the Near East. Stevanovic (1997) estimated that intentional house burning could attain temperatures in excess of 1000 °C. Tringham (2005) further discusses this phenomenon. In Turkey, finds of vitrified building earth associated with house burning have been reported from the Neolithic Çatal Höyük (Çatalhöyük Archive Reports 2005 and 2011) and at the Bronze Age site of Tilmen Höyük (Marocchi et al., 2010).
4) Another form of melted silica has been found on archaeological sites and was studied in Israel. Here silicic melt was formed by fusion of cereal straw or chaff (Folk and Hoops, 1982). This phenomenon has been observed also today where straw or haystacks have burned or when intense grass-fires occurred (Baker, 1968). Ash and slag of plant material can be identified by their compositions (Thy et al., 2013a). In addition to generally high SiO_2, plant ash is identified by high K_2O, wood ash in addition by high CaO, whereas in soils and sediments Al_2O_3, Na_2O, and Fe_2O_3 will variably predominate. Similar finds of siliceous slag-like material have been found in Anglo-Saxon cremation urns at the sites of Elsham and Illington in England where chemical analyses suggest that the surrounding sediment had melted (Henderson et al., 1987).
5) Finally, highly vesicular, siliceous scoria droplets, which are the subject of this report, are common on archaeological sites in northern Syria. So far the only reports on these are by Bunch et al. (2012) and Wittke et al. (2013), who suggest that they were the result of a cosmic impact. Despite scarce reports on scoria droplets they are well known to archaeobotanists because they are easily collected by water flotation.

The evidence outlined above demonstrates that conditions capable of melting building earth prior to the invention of draught kilns occurred on archaeological sites. Off-site burning may also likewise cause melting. In Australia there are reports of bush fires producing silica-rich slag (Baker and Gaskin, 1946; Humphreys et al., 2003). Ignition of surface exposed coal seams is another natural event that can produce glass-containing clinkers and scoria (Stracher, 2007). It should also be considered that glass is a common product or by-product of metal smelting, iron smithing, ceramic and glass making, as well as a natural phenomenon associated with volcanic eruptions (glassy lava, scoria, and tephra). Thus contamination from such sources must be considered. The sites reported here are dated several millennia before the invention of ceramics and smelting and are located far from any volcanic activity.

One of the reasons that archaeologists apparently have ignored the presence of scoria objects until recently is due to the perceived impossibility that fires on ancient settlements could reach high enough temperatures to melt silica-rich earth material and soils. Although it may be surprising, there are indications that silica-rich materials can melt at relatively low temperatures and that temperatures of house fires may be higher than previously assumed. The melting temperature of pure silica, or quartz polymorphs, is 1723 °C. However in multi-component systems characterized by high SiO_2 content, this melting temperature will be greatly reduced by the presence of other oxides, particularly of alkali metals such as K_2O and Na_2O, resulting in initial melting occurring often well below 1000 °C (Schairer, 1957; Levin et al., 1964; Muan and Osborn, 1965; Shelby, 2005). The melting rate and reactivity of silica-rich material are in addition governed by the grain-size and homogeneity of the reactants, so fine well-mixed dust will melt more readily. Industry takes advantage of this by fabricating a paste of silica dust combined with various compounds known as glass frit which sinter at temperatures below 500 °C. Earth used for the construction of buildings is often made up of fine eolian sediments and/or soil, which when combined with a cocktail of organic compounds present in or near habitations could easily result in silica-rich materials with low initial melting temperatures in the range from 800 to 1000 °C.

Temperatures in house fires are often quoted as not normally reaching temperatures much above 500 °C. However, experiments carried out by fire safety experts show that compartment fires with a source of ventilation such as an open door or window causing a draught can lead to temperatures in excess of 1000 °C (Fleischmann and Parkes, 1997). In experimental room fires, temperatures peaked at between 1000 °C and 1100 °C. (Klopovic and Turan, 2001). According to Bryan (1980), a fire safety scientist, fire-storms create massive flames with temperatures ranging from 500 to 1000 °C. Given the above evidence, it is plausible that temperatures could be attained which could partially melt siliceous sediments in ancient settlements, especially in view of the fact that highly flammable combustibles in the form of stockpiles of cereal chaff, straw, and dry wood would have been abundant in, on, or beside buildings (Willcox and Stordeur, 2012).

In the present contribution, we present analyses on archaeological scoria droplets from pre-ceramic sites dating to the terminal Pleistocene and Early Holocene of the Near East, indicating that these must be considered alongside the example above as deriving from on-site fires, and not from an extraterrestrial impact.

2. Materials and ages

Information on settlement phases and radiocarbon dates of levels within the archaeological sites, which provided scoria and vitrified building earth, are given in Table 1. The approximate age range of the levels sampled for this study was based on multiple determinations obtained from the listed references. Site locations are shown in Fig. 1.

Scoria droplets selected for this study were taken from products of water flotation, those from Abu Hureyra by D.Q. Fuller at the Institute of Archaeology at University College London (UCL) and those from the other sites by G. Willcox at Jalès, Archéorient CNRS in France. Flotation sampling is a standard method for recovering charred plant material. The reason that scoria float is due to their vesicular nature. Samples used in the studies by Wittke et al. (2013) and Bunch et al. (2012) were obtained from the same collection at UCL. Records of scoria consist of eight flotation samplings from Jerf el Ahmar, three from Dja'de and four from Tell Qaramel. These were found in layers with ash and charcoal and were in some cases associated with buildings destroyed by fire, perhaps intentionally.

Table 1
Summary of examined scoria droplets from northern Syrian sites.

Site		Phase	Level	Date		EMP	LA-ICPMS
Abu Hureyra 1	Silicate scoria	1	470 (73/326)	13,200 – 13,000	Moore et al., 2000	Glass	
Abu Hureyra 1	Silicate scoria	2	427 (73/283)	13,000 – 12,500	Moore et al., 2000	Glass	
Abu Hureyra 1	Silicate scoria	3	412 (73/268)	12,300 – 11,500	Moore et al., 2000	Glass	
Abu Hureyra 1	Silicate scoria	3	402 (73/258)	12,300 – 11,500	Moore et al., 2000	Glass	Glassy matrix
Qaramel	Silicate scoria	H2	45/1657	12,300 – 11,500	Mazurowski and Kanjou, 2013	Glass	Glassy matrix
Jerf el Ahmar	Silicate scoria A,B	6	651/A95/D91	11,200 – 10,800	Stordeur and Abbes, 2002	Glass	Glassy matrix
Jerf el Ahmar	Silicate scoria A,B	6	653/A95/D95	11,200 – 10,800	Stordeur and Abbes, 2002	Glass	Glassy matrix
Dja'de	Silicate scoria	3	CY/3	10,500 – 10,200	Coqueugniot, 2000	Glass	Glassy matrix
Mureybet	Building earth	IIIA	Building 47	11,300 – 10,800	Ibañez, 2008	Fine matrix	
Abu Hureyra 1	Silicate scoria	2	445	13,000 – 12,500	Bunch et al., 2012, Wittke et al., 2013		

Scoria droplets from Abu Hureyra 1, level 445, were analyzed by Bunch et al. (2012) and Wittke et al. (2013).

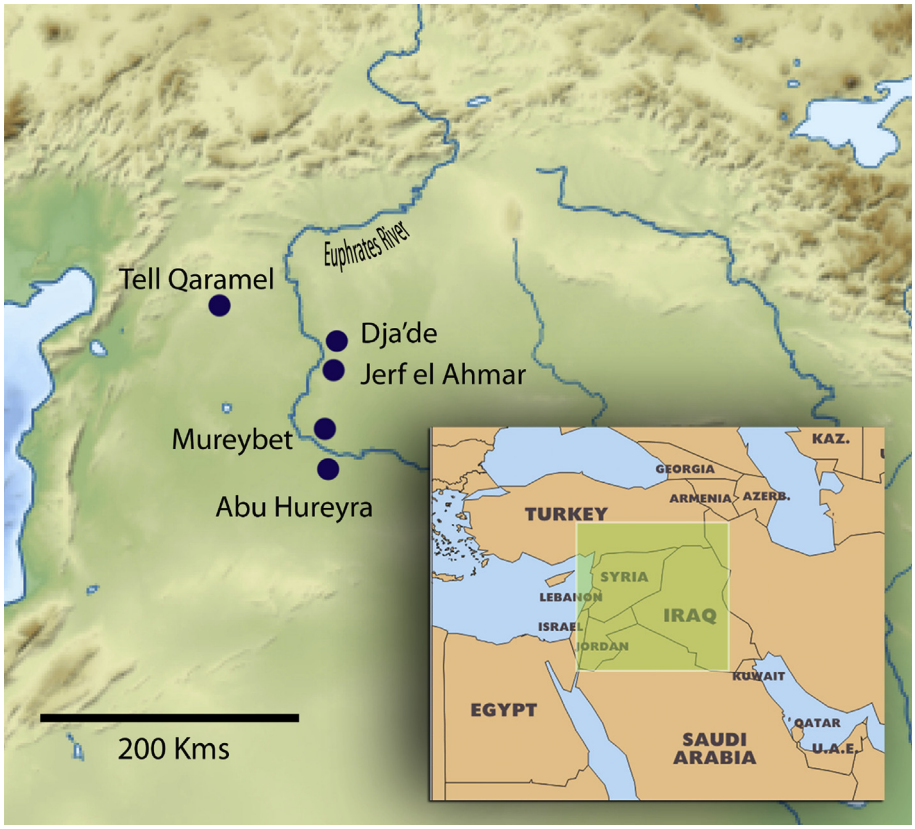

Fig. 1. Summary locations of the examined Syrian archeological sites where silicious scoria were found.

Intense burning was noted from cracked bricks and reddened earth, which in at least two cases was vitrified. Scoria was not consistently present in the sediments and there is no reliable data on their frequency. They appear to be relatively infrequent, probably because conditions for their formation were rare. In many cases, scoria, however, may have been disregarded because sorting was not aimed at their recovery. An example of the latter is at the site of Shillourkambos dated to about 10,500 year ago on the island of Cyprus where scoria droplets were found, but were not reported (Willcox, 2011).

Abu Hureyra 1 is a hunter-gatherer site dating to the end of the Pleistocene. Occupation corresponds approximately to the Younger Dryas. Possible pre-domestic cultivation was proposed (Hillman et al., 2001), but was recently refuted by Colledge and Conolly (2010). The studied samples from the multi-period site at Qaramel came from a level dated from the end of the Younger Dryas to the beginning of the Holocene (Willcox and Herveux, 2013). Dates at Jerf el Ahmar correspond to the beginning of the Holocene, when the climate became more favourable. There are signs of cultivation, but no morphological domestication. Finally, the sample from Dja'de came from levels dated to 1000 years after the Younger Dryas. The economy was probably similar to Jerf el Ahmar (Willcox et al., 2008).

In summary the scoria analyzed come from levels dated approximately to between 10,200 and 13,200 years ago and thus span about 3000 years. We found no evidence to suggest that they concentrated at the beginning of the Younger Dryas (~12,900 years ago).

3. Methods

Scoria droplets and fragments (Table 1) were mounted under vacuum in epoxy, sectioned, and polished for scanning electron microscopy, electron beam, and laser ablation analyses. Two

horizons were sampled in duplicates (Jerf el Ahmar). Only those that contained sufficient glass or fine-grained matrix for quantitative analyses are discussed in details.

A CAMECA SX-100 electron microprobe (EMP) was used for the study equipped with five wavelength dispersive spectrometers (WDS) and high speed and high-resolution, back-scattered electron (BSE) imaging facilities. Light microscopy and BSE images were used to evaluate the scoria particle form and their internal fabric and to locate clean glass for quantitative WDS spot analyses. The analytical conditions, in part selected to minimize loss of sodium, were an acceleration voltage of 15 kV, a beam current of 7 nA, peak counting times of 10 or 20 s, and a 5 μm raster length. Some fine-grained matrix analyses were done with a raster size of 20 μm. All phases were analyzed using natural minerals and glasses as standards. Two internal volcanic glass standards (VG-2, Thornber et al., 2002; VG-568, Rowe et al., 2008) were analyzed concurrently as a control and measure of precision and accuracy (Table 2). The analytical precision is typically 1–3 % for major oxides and increases for low concentration oxides to 5% or above, with a lower limit of detection for the latter at 0.01 wt. %. The results are reported as averages and the standard deviation at the 1σ level for each site or horizon giving all iron as total Fe_2O_3. The proportion of ferric and ferrous iron in air in the glasses was estimated using the equations of Kilinc et al. (1983) and Volovetsky et al. (2010) at approximately 0.15 FeO/Fe_2O_3. These recalculated values are used for comparison with analogue ternary phase diagrams. Representative analyses of minerals are given in Inline Supplementary Table 1.

Inline Supplementary Table 1 can be found online at http://dx.doi.org/10.1016/j.jas.2014.11.027.

Laser ablation, inductively coupled plasma, mass spectrometry (LA-ICP-MS) analyses for a suite of trace elements were done using a Agilent Technologies 7500a quadrupole ICP-MS coupled to a New Wave Research UP-213-nm laser using He as the carrier gas. Laser parameters were set at 70% energy, 10 Hz pulse frequency, and 80-μm diameter spot size. The measurements from three replicate scans in the glass-rich parts of droplets were then done as 300-μm line-scans. Data was acquired for 50 s following 25 s background analysis. We quantified isotopes of 44 elements with Glitter, the GEMOC Laser ICP-MS Total Trace Element Reduction software package, using USGS synthetic glass standard GSD-G1 as the calibration standard (with the exception that GSE-1G was used for platinum) and by matching the ^{43}Ca counts to the CaO concentrations obtained on the sample glasses by electron microprobe (Table 2). GSE-1G was used as internal standard (Inline Supplementary Table 2).

Inline Supplementary Table 2 can be found online at http://dx.doi.org/10.1016/j.jas.2014.11.027.

Thermogravimetric (TG) analysis was done on a finely ground, slightly burnt building earth from Mureybet (III 27) using a PerkinElmer Diamond TG/DTA Analyzer. A total of 30 mg powder were placed in an open alumina crucible and heated in purge air with a 200 ml min^{-1} flow rate and constant heating rate of 10 °C min^{-1} from initial ambient temperature up to a final temperature of 1200 °C. Temperature and heat flow calibrations were done using the melting points of indium and gold.

Thermodynamic modelling of the melting behaviour and melt composition was investigated using Gibbs free-energy minimization and the FactSage thermochemical software and solution

Table 2
Electron microprobe analyses of glass phase in scoria droplets from northern Syria.

ID/Oxide	Abu Hureyra 1		Abu Hureyra 1		Abu Hureyra 1		Abu Hureyra 1		Qaramel		Jerf el Ahmar		Jerf el Ahmar	
	470 (73/326)		427 (73/283)		412 (73/268)		402 (73/258)		45/1647		651/A95/D91 (A)		653/A95/D95 (A)	
	Av ($N = 4$)	STD	Av ($N = 5$)	STD	Av ($N = 5$)	STD	Av ($N = 5$)	STD	Av ($N = 6$)	STD	Av ($N = 7$)	STD	Ave ($N = 6$)	STD
SiO_2	54.37	0.93	54.62	1.76	58.48	0.76	48.45	1.55	49.04	0.98	47.93	1.03	48.60	1.16
TiO_2	0.70	0.10	0.59	0.07	0.74	0.04	1.04	0.11	1.36	0.22	1.03	0.12	0.95	0.08
Al_2O_3	10.10	0.97	9.36	0.55	10.15	1.16	13.78	0.23	13.85	0.79	14.39	0.30	10.87	0.85
Fe_2O_3	7.21	0.83	5.55	0.67	5.32	0.34	9.62	1.02	10.26	1.27	7.28	1.32	6.96	0.60
MnO	0.17	0.02	0.10	0.01	0.13	0.04	0.15	0.01	0.19	0.01	0.15	0.03	0.14	0.01
MgO	2.84	0.66	5.40	0.85	5.11	0.27	6.74	0.54	4.47	0.46	7.39	0.46	6.82	0.36
CaO	17.87	0.11	18.78	1.12	14.80	0.66	17.62	2.56	19.92	1.50	19.40	1.25	20.03	0.81
Na_2O	2.98	0.20	2.21	0.12	2.38	0.38	1.40	0.24	0.31	0.11	1.41	0.18	1.72	0.15
K_2O	2.88	0.19	3.08	0.48	2.92	0.16	1.40	0.23	1.53	0.39	2.21	0.50	2.29	0.28
P_2O_5	0.87	0.06	0.97	0.11	0.42	0.05	0.56	0.12	0.57	0.08	0.23	0.11	0.77	0.17
Cr_2O_3	0.02	0.01	0.03	0.01	0.03	0.01	0.03	0.01	0.05	0.03	0.04	0.02	0.03	0.02
NiO	0.02		0.02	0.02	0.04	0.01	0.05	0.01	0.04	0.02	0.07	0.03	0.04	0.04
Cl	0.01		0.01		0.01	0.00	0.01	0.00	0.02	0.01	0.03	0.02	0.01	0.01
Total	100.03		100.71		100.53		100.86		101.58		101.53		99.23	

ID/Oxide	Jerf el Ahmar		Jerf el Ahmar		Dja'de		Mureybet		Rhyolite			Basalt		
	651/A95/D91 (B)		653/A95/D96 (B)		CY3		Build 47		VG-568			VG-2		
	Av ($N = 5$)	STD	Av ($N = 5$)	STD	Av ($N = 5$)	STD	Av ($N = 6$)	STD	Av ($N = 6$)	STD	Recomm.	Av ($N = 6$)	STD	Recomm.
SiO_2	46.52	1.01	47.63	0.67	50.84	0.97	50.28	1.49	77.35	0.25	76.55	50.82	0.30	50.81
TiO_2	0.92	0.11	1.01	0.09	0.84	0.16	0.95	0.21	0.09	0.02	0.08	1.89	0.04	1.89
Al_2O_3	11.78	0.47	12.39	0.46	8.80	0.89	16.38	1.48	12.40	0.09	12.44	14.19	0.11	14.00
Fe_2O_3	7.96	0.32	7.50	0.48	6.22	0.55	5.80	0.51	1.26	0.09	1.11	13.04	0.15	13.15
MnO	0.16	0.06	0.16	0.01	0.14	0.02	0.09	0.03	0.03	0.03	0.02	0.21	0.02	0.21
MgO	7.26	0.32	6.43	0.21	5.72	0.26	4.79	0.73	0.04	0.01	0.03	7.08	0.09	6.66
CaO	21.28	0.78	20.50	0.86	21.86	0.80	16.84	0.97	0.41	0.04	0.39	11.02	0.17	11.06
Na_2O	1.56	0.15	1.90	0.18	1.70	0.09	2.42	0.29	3.38	0.30	3.51	2.61	0.05	2.62
K_2O	1.94	0.27	1.74	0.17	2.08	0.27	1.90	0.29	4.81	0.08	4.91	0.20	0.01	0.19
P_2O_5	1.10	0.16	0.86	0.12	2.13	0.71	0.17	0.07	0.01	0.01	0.01	0.23	0.01	0.20
Cr_2O_3	0.03	0.01	0.04	0.01	0.05	0.02	0.02	0.00	nd			0.03	0.01	
NiO	0.04	0.02	0.04	0.04	0.04	0.02	0.06	0.03	0.01	0.01		0.02	0.02	
Cl	0.01	0.01	0.01	0.01	0.03	0.01	nd		0.11	0.01	0.12	0.03	0.00	
Total	100.56		100.21		100.41		99.68		99.79	0.92	99.05	101.35		100.79

Av – averaged; N – number of analyses; STD – standard deviation; nd – not detected; Recomm. – recommended values.
Basalt VG-2 – Juan de Fuca basalt glass (Thornber et al., 2002). Rhyolite VG-568 – rhyolite glass from Mount St. Helens 2004–05 tephra (Rowe et al., 2008).

databases (Bale et al., 2002). An average of glass analyses in scoria droplets (Table 2) was used to model melting/crystallization at atmospheric conditions with FactSage and a silicate solution model without gas and salt modelling.

4. Results

4.1. Scoria shape and texture

Charcoal, ash, and building earth fragments affected by heating are common on all the discussed Syrian sites (e.g. Moore et al., 2000). Evidence of direct melting, however, is less common. Decimeter large cinder fragments of burnt and partially melted building earth were nevertheless found at the two sites Jerf el Ahmar and Mureybet. The latter was available for analysis (Fig. 2A). This composite example varies from burnt earth (left) to expanding, highly vesicular and convoluted surfaced scoria (right). The interior of the melted earth is highly vesicular pumice with minute to millimeter-sized, coalesced to irregular air bubbles in a matrix of mostly fine-grained material (Fig. 2B). The matrix contains little preserved glass, but occasional fine-grained parts allow the matrix to be analyzed using a large raster size with the EMP. Scoria is sometimes pervasively altered to secondary clay minerals by percolating water that is also recorded by precipitated hydroxides and carbonates on inside vesicle walls (Fig. 2C).

The sites examined (Table 1) contain scoria droplets and fragments ranging in size from <1 mm to >10 mm (Fig. 3). The outer form varies from irregular elongated (Fig. 3A), rounded (Fig. 3E), coalescence or dumbbell shaped (Fig. 3G), and tear-shaped droplets (Fig. 3C, D, H). Fragments are found clearly revealing a thin (<0.5 mm) siliceous walls surrounding single large bubbles (Fig. 3A, I) and examples of bubbles that have burst through the thin wall can be observed (Fig. 3A, G). Some droplets show signs of precipitation of hydroxides and carbonate on inner vesicle surfaces (Fig. 3B; see also Fig. 2C) and also carry straw-type ash particles embedded in the surface or in some cases penetrating walls without showing clear sign of melting (Fig. 3B, H).

Representative mean-atomic density or back shattered electron maps (BSE) are shown in Fig. 4. There are three main features worth discussing. (1) Melt or evidence of melt is present in all investigated scoria fragments (Fig. 4C, F). The silicate melt is preserved during cooling as a glass and is in contact with vesicles and partially reacted mineral grains (Fig. 4C–F). The amount of glass varies from being dominating (Fig. 4F) to local in an interstitial fabric or replaced by secondary grown and annealed grains (Fig. 4G). (2) Gas bubbles (or vesicles) are pervasively present and range from irregular large shapes dominated in parts by bubble coalescing and the

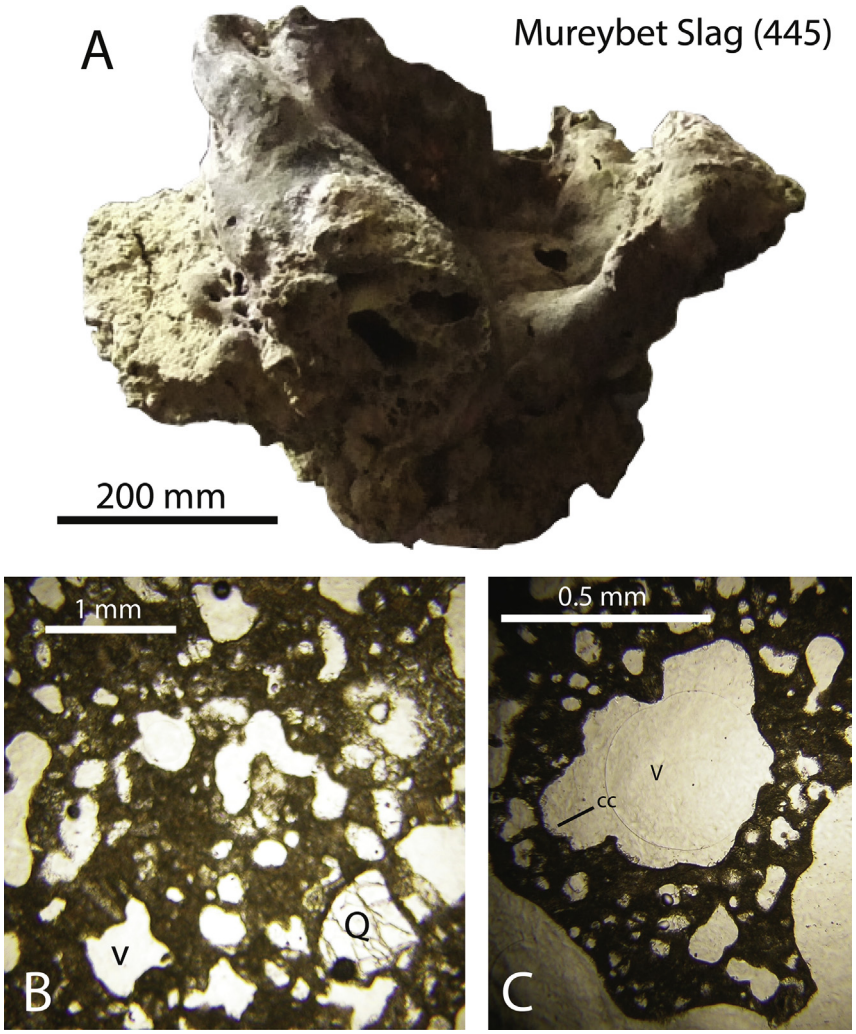

Fig. 2. Building earth fragment (Mureybet 445). (A) Increasing melting from left to right shown by vesiculation and flow contortion. Scale bar is 200 mm. (B) Irregular vesicles (V) and quartz grains (Q) in a complex crystalline matrix. Scale bar is 1 mm. (C) Central large irregular vesicle (V) with precipitated carbonate crystals (cc). Scale bar is 0.5 mm.

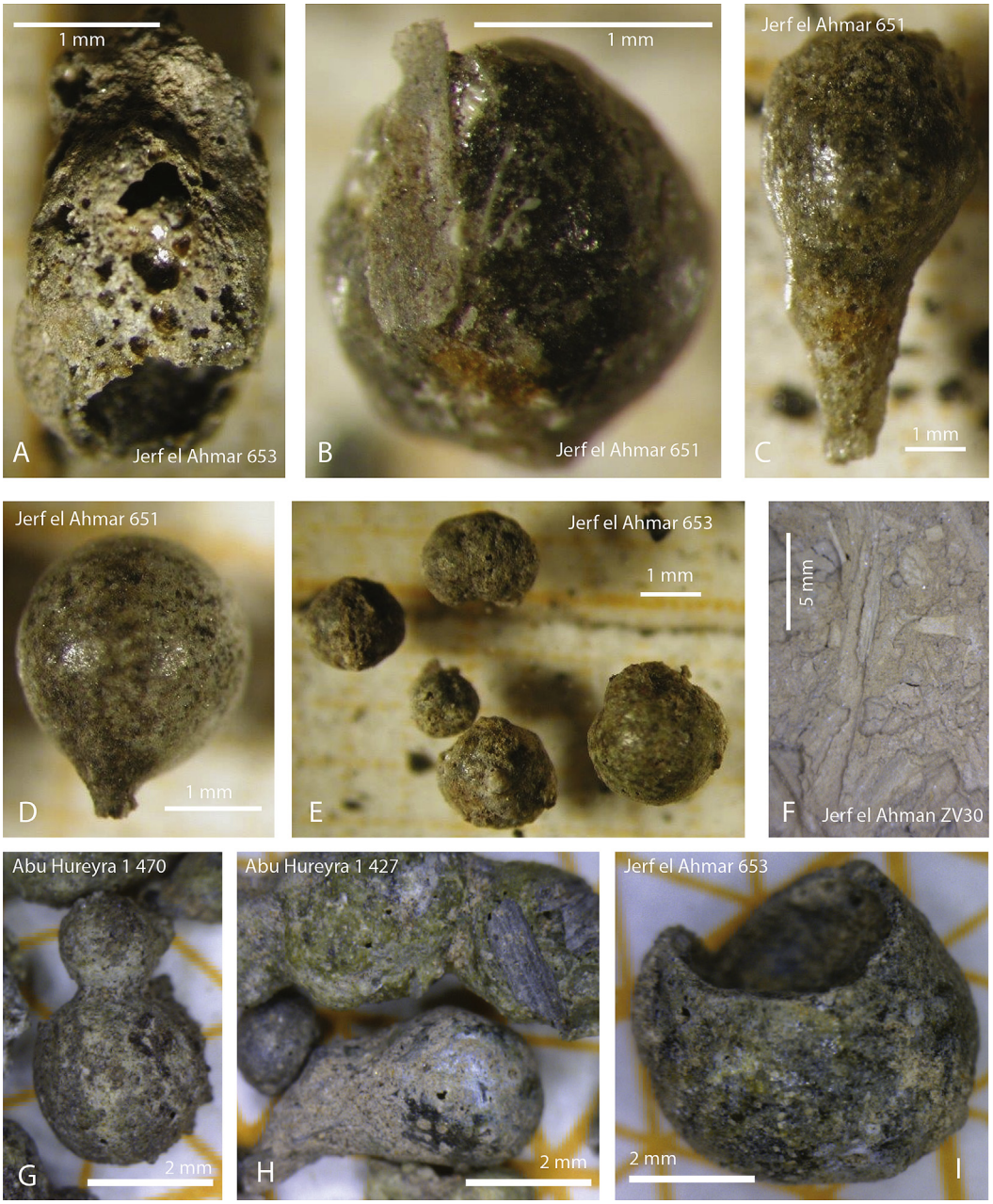

Fig. 3. Typical morphologies of scoria droplets and fragments. (A) Elongated scoria fragment from Jerf el Ahmar 653. (B) Circular scoria from Jerf el Ahmar 651 with adhering straw ash fragment. (C) Teardrop shaped scoria from Jerf el Ahmar 651. (D) Near round scoria droplet with rudimentary elongation at the bottom from Jerf el Ahmar 651. (E) Small near round droplets from Jerf el Ahmar 653. (F) Surface of block of building material from Jerf el Ahmar ZV30 with abundant imprint on the surface of plant straw fragments. (G) Dumbbell shaped scoria droplet from Abu Hureyra 1470. (H) Irregular shaped droplets from Abu Hureyra 1427 with several adhering straw ash fragments. (I) Broken droplet exposing large internal vesicle and thin wall from Jerf el Ahmar 653. Scale bars are 1 mm (A–E), 5 mm (F), and 2 mm (G–I).

presence of relict minerals in the silicate walls (Fig. 4A, E, G) to perfect smaller rounded shapes often found in areas dominated by glass (Fig. 4C, F). These types of vesicles are very similar to those found in volcanic eruptive scoria resulting from the release of gasses during melting, bubble growth, and exsolution during cooling of the melt until frozen by the glass transition (Heiken and Wohletz, 1985; Cashman and Mangan, 1994). They are thus clear signs of melting, cooling, and the presence of an original significant volatile component. (3) Skeletal crystal are often present suggesting nucleation from the melt and growth during cooling (Fig. 4A, B, H).

The mineralogy is largely consistent among the scoria dominating mainly by feldspars (plagioclases and orthoclase) in various stages of dissolution (Fig. 4C–F), large quartz grains either partially or largely undissolved (Fig. 4C–F), diopsidic pyroxene or wollastonite and plagioclases dominating among the quench phases (Fig. 4H), irregular to subhedral chromian spinel grains (Fig. 4D–F), and occasionally a droplet-shaped goethitic hydroxide (Fig. 4E). Other minerals detected include apatite, rutile, carbonate, and sulfate. The basic observation from the melt–mineral relations is indication for preferential melting of a mixture of a fine-grained matrix with larger grains (feldspars and quartz) only partially melted and reacted. The melting process is thus one of heterogeneous disequilibrium resulting from low temperature, short heat source duration, and fast cooling.

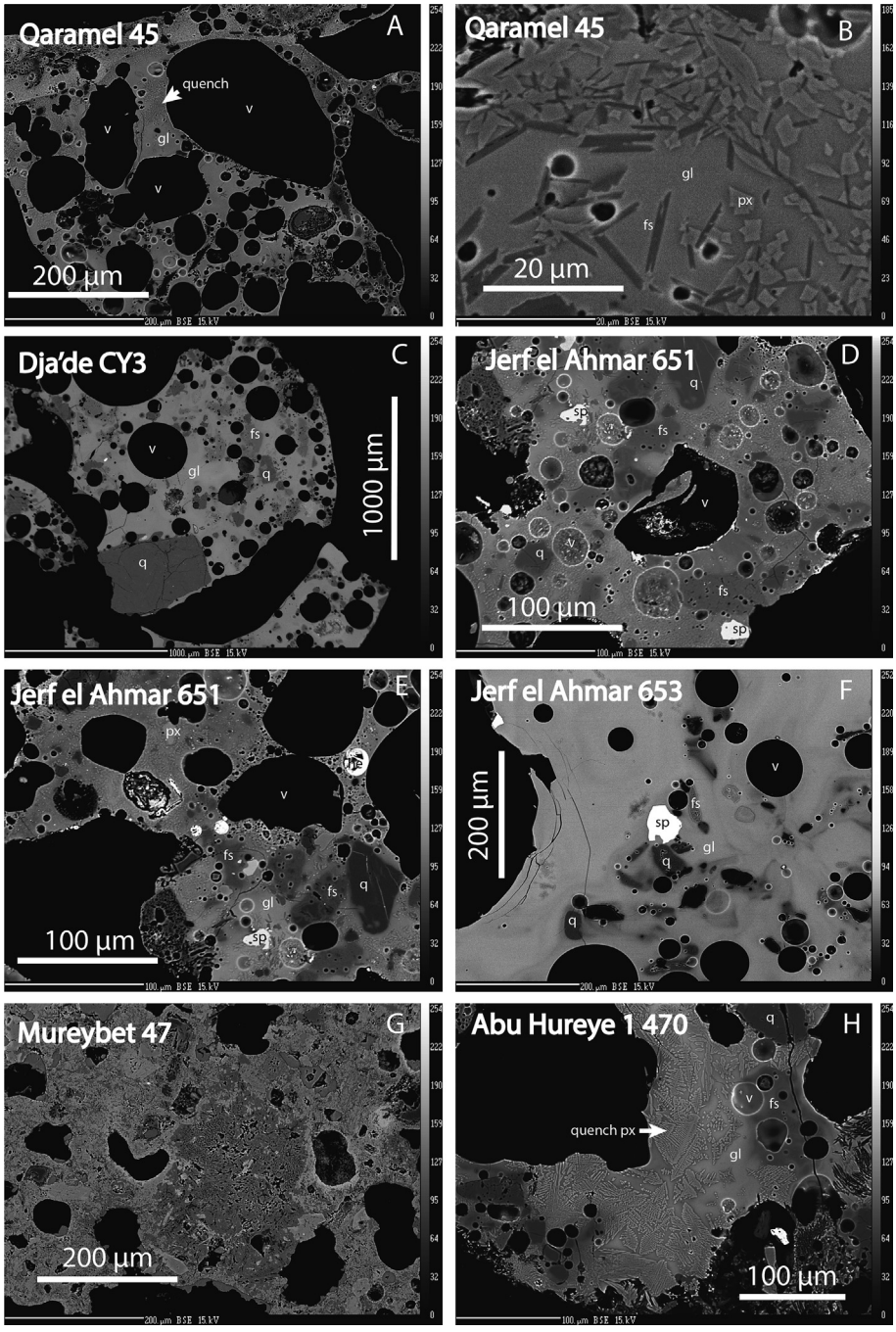

Fig. 4. Representative SEM images as back-scattered, mean-atomic, density maps. (A) Fragment from Qaramel 45 with highly variable sized vesicles and quench pyroxenes and feldspars in a glass matrix. Scale bar is 200 µm. (B) Close-up of the quenched area from (A) showing feldspar and pyroxene. Scale bar is 20 µm. (C) Fragments from Dja'de CY/3 with broken surfaces controlled by vesicle shapes. Scale bar is 1000 µm. (D) Fragment with vesicles (often filled by epoxy) from Jerf el Ahmar 651. Scale bar is 100 µm. (E) Fragment from Jerf el Ahmar 651 with large irregular vesicles and unreacted quartz and feldspar grains. Scale bar is 100 µm. (F) Fragment from Jerf el Ahmar 653 dominated by glass with partial melted quartz and feldspars and a central large spinel. Scale bar is 200 µm. (G) Fragment from Mureybet 47 (see Fig. 2) with irregular vesicles in a crystalline fine-grained matrix without detectable glass. Scale bar is 200 µm. (H) Fragment from Abu Hureyra 1 470 with quench skeletal pyroxenes in a matrix of glass together with large unreacted quartz and feldspars. Scale bar is 100 µm. Abriaviations are v (vesicle), q (quartz), gl (glass), fs (feldspars), and sp (spinel).

4.2. Glass and mineral compositions

The glass is composed of, in order of decreasing amount, SiO_2, CaO, Al_2O_3, Fe_2O_3, MgO, K_2O, Na_2O, TiO_2, and P_2O_5, although considerable variations are observed between locations (Table 2). The dominating SiO_2 and Al_2O_3 (~60%) explain the ease with which the melts form glass during cooling. The most consistent feature is the relatively high CaO content (15–22 wt. %) and also the dominance of K_2O over Na_2O for most analyses. The total concentration of the main oxides (CaO, Al_2O_3, and SiO_2, representing about 80% of the total mass) is illustrated on binary variation diagrams in Fig. 5. The scoria glass compositions from the Syrian locations show considerable variation in Al_2O_3 and CaO with more restricted variation in SiO_2. Including the analyses by Bunch et al. (2012) and Wittke et al. (2013), the total range is extended toward higher CaO and lower Al_2O_3 (Fig. 5). The inter-variation is considerably larger

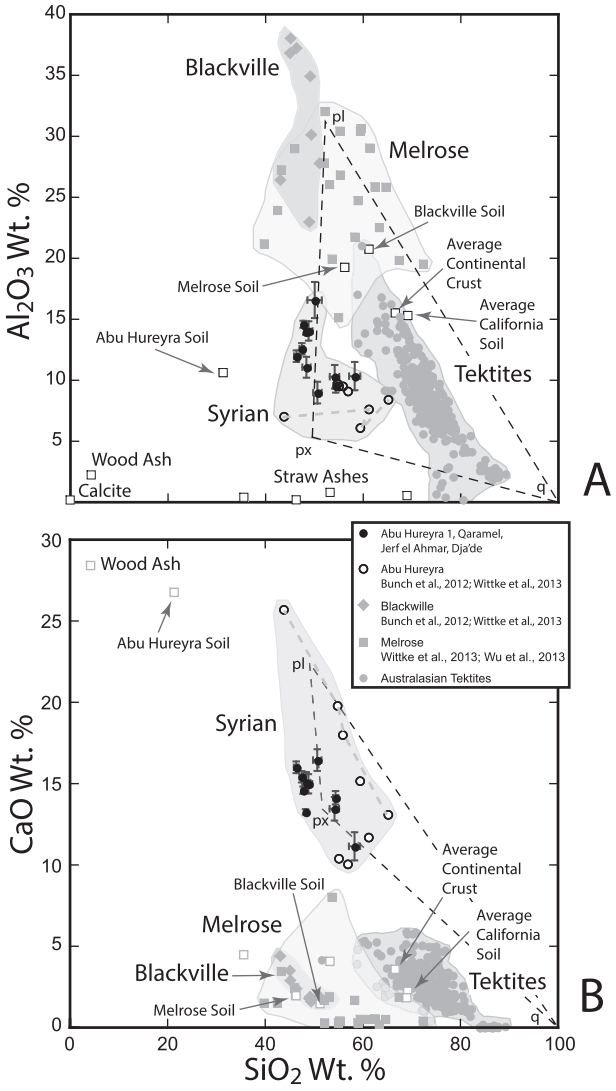

Fig. 5. Binary oxide variation diagrams with SiO_2 (wt. %) as the abscissa. (A) Al_2O_3 wt. %. (B) CaO wt. %. Shown is the Syrian glass compositions (Table 2) together with those reported by Bunch et al. (2012) and Wittke et al., 2013; Blackville and Melrose scoria compositions reported by Bunch et al. (2012), Wittke et al. (2013), and Wu et al. (2013); Australasian tektites (O. Stecher, personal communications, 2014); local soil compositions from Abu Hureyra, Blackville, and Melrose from Bunch et al. (2012); average California soil and continental crust from Bradford et al. (1996) and Rudnick and Gao (2003), respectively; wood and various straw ashes from Thy et al. (2013a). Stippled black lines connect the main silicate minerals found in the Syrian droplets (pl, plagioclase; q, quartz, and px, pyroxene). Stippled grey line connects the droplet profile analyzed by Wittke et al. (2013).

than the intra-variation suggesting that local heterogeneities in the melting source in part controlled the scoria compositions. Wittke et al. (2013), however, analyzed four points across the same scoria and saw considerably variation in CaO for a single droplet (Fig. 5), suggesting that the overall variation seen for the droplets at least in part can be attributed to heterogeneities in the droplets.

The observed minerals coexisting with the melt (or glass) are dominated by feldspars and quartz (Inline Supplementary Table 1). The feldspars vary in composition from plagioclase (Ca- and Na-rich) to orthoclase (K-rich) with reasonable, although not perfect, stoichiometry ($Z = 4$, $X = 1$, $O = 8$; Inline Supplementary Table 1). The pyroxene is diopsidic with equal partitioning of alumina between tetrahedral and octahedral positions, high ferric iron content, and unusual high wollastonite (or Ca-content) compared to common terrestrial pyroxenes. The spinel in the Jerf el Ahmar droplets (Fig. 4D–F) is a magnesioferrite-magnesiochromite spinel with ferric iron dominating over ferrous. The iron-rich spherules seen in some droplets (Fig. 4E) are likely secondary iron hydroxides fillings of vesicles (goethite, limonite) (Inline Supplementary Table 1). The dominating ferric iron in diopside and spinel confirms the assumption that most iron in the droplets equilibrated in air.

4.3. Trace element composition

The trace element composition of the scoria droplets potentially provides important fingerprinting of their origins (soil type, residuals from organic material, cosmic tracers). With this in mind, we analyzed the siliceous scoria walls using laser-ablation. Despite the fact that all analyzed scoria walls contain glass, the heterogeneity of the material prohibited determination of the composition of pure glass, as done for the major element compositions (Table 2). The analytical results, because of the sizes of the used line scans and the inability readily to identify individual minerals and glass patches, thus represent the average composition of the scoria walls. Average trace element compositions and standard deviations are summarized in Inline Supplementary Table 2 as well as in Fig. 6.

Particular emphasis was made to detect the platinum-group elements (PGE) because they potentially may record an even small amount of extraterrestrial addition (Evans et al., 1993; Koeberl, 2007). The only two PGEs for which useful standards were available were, however, systematically below detection limits (Ir < 0.018 ppm and Pt < 0.076 ppm) in all cases, and thus no positive impact component could be detected.

The average scoria trace element composition (with some additional major elements) is shown in a semi-logarithmic diagram in Fig. 6 normalized to an estimated global average continental crust (Rudnick and Gao, 2003) and organized as a function of increasing atomic number (Z). The normalization against a common reference composition allows the identification of site-specific characteristics of the soil (or complex source) composition. The scoria contains elevated concentrations of most of the alkali earth elements (Mg, Ca, Sr) and slightly lower concentrations of the alkali metals (Li, Na, K, Rb, Cs). Of the transition metals, Cr and Ni are elevated, while Zn is depleted. Most noticeable, Cd is elevated to ~10 times continental crust (with the exception of two measurements) where the Cd concentrations were found to be below the detection limit (<0.06 ppm, Inline Supplementary Table 2). Other elements that show large variations likely due to the heterogeneous nature of the scoria walls are As, Sn, Cs, and Pb, as reflected in their large standard deviations (Fig. 6). The rare earth elements (REE) show systematic increasing normalized variations with increasing atomic number (Z) through the series from La to Yb as commonly observed for soils (Gustavsson et al., 2001; Rudnick and Gao, 2003; Tyler, 2004); reflecting the similar chemical behaviour of all the REEs as well as the underlying geologic foundation.

4.4. Analogue ternary liquidus surface

Correlations between direct fusion, thermodynamic modelling, and simplified silicate liquidus phase diagrams have often been demonstrated for silicate ash and slag in combustion boilers (Huggins et al., 1981; Kalmanovitch and Williamson, 1986; Gray, 1987; Seggiani, 1999; Bryant et al., 2000; Jak, 2002) as well as for archaeological problems (e.g. Rehren, 2000). Direct application of simplified liquidus phase diagrams without appropriate calibration for multi-component compositions, such as the scoria compositions investigated here, may however at the best only provide relative temperature estimates (e.g. Bunch et al., 2012; Wittke et al., 2013).

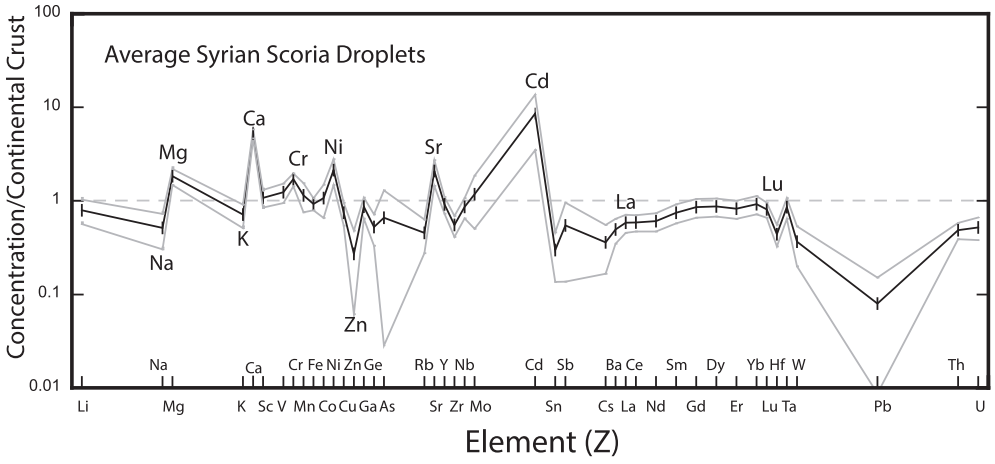

Fig. 6. Elemental compositions for selected major and trace elements detected in the droplets normalized to continental crust (Rudnick and Gao, 2003) and shown on semi-logaritmic diagram against the atomic number in the periodic system (Z). Heavy line is the average composition from Inline Supplementary Table 2 and the thin grey lines are the total variation in the 1σ standard deviation.

The compositions of the Syrian scoria are dominated by SiO_2, Al_2O_3, and CaO (~80% of the total mass) and the ternary liquidus phase diagram CaO–Al_2O_3–SiO_2 (CAS; Muan and Osborn, 1965) may thus provide some insight into the melting behaviour and crystallization of the scoria droplets (Fig. 7). The glass compositions of Table 2 cluster mostly around the binary cotectic defined by anorthite and wollastonite and approach the minimum eutectic melting point (1170 °C), adding quartz to the mineral assemblage. The glasses analyzed by Bunch et al. (2012) and Wittke et al. (2013), together with three analyses of this study, cluster away from the eutectic point mostly suggesting higher temperatures of 1300–1500 °C. The present results, nevertheless, indicate that most of the scoria glass formed at binary cotectic and eutectic melting relations down to a temperature of 1170 °C in equilibrium with anorthite, wollastonite, and/or tridymite. These mineral phases are the simplified CAS analogues of the silicate minerals observed in the scoria (quartz, feldspar, diopside). The estimated minimum melting temperature of 1170 °C may nevertheless represent a maximum since it does not consider the effects of the remaining 20% of the mass,

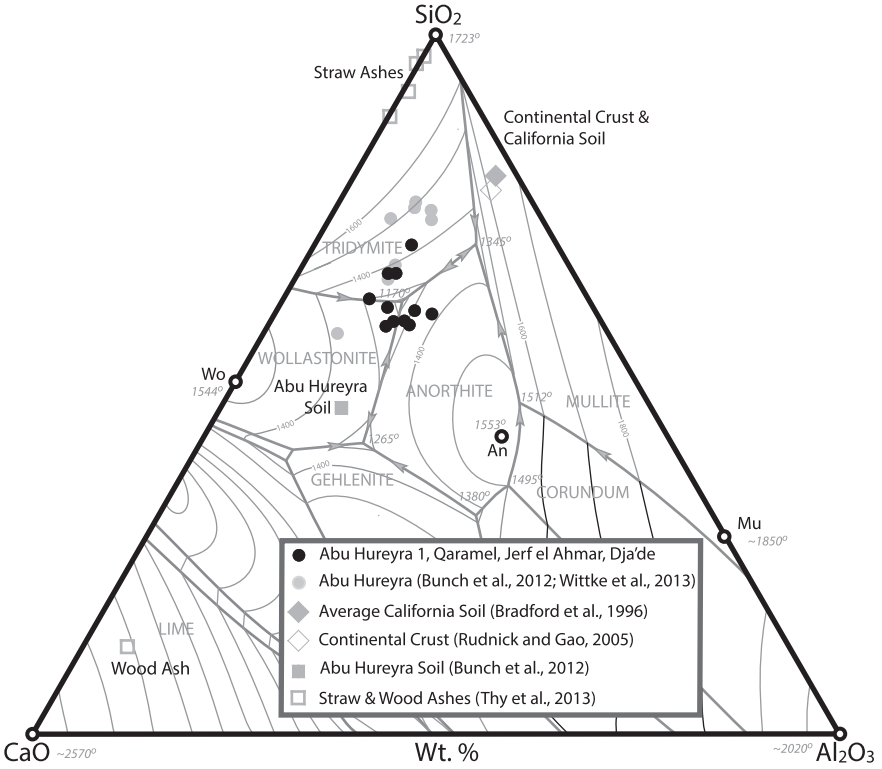

Fig. 7. Part of the simplified liquidus surface in the CaO–Al_2O_3–SiO_2 ternary diagram from Muan and Osborn (1965). Shown is the liquidus surface contoured for temperature, univariant lines with arrows indicating decreasing temperature and the eutectic and peritectic points with temperatures in italic. The data plotted is the Syrian glass compositions (Table 2) together with those reported by Bunch et al. (2012) and Wittke et al., 2013; local soil compositions from Abu Hureyra by Bunch et al. (2012); average California soil from Bradford et al. (1996); continental crust from Rudnick and Gao (2003); and wood and straw ashes from Thy et al. (2013a). The locations of the main mineral phases of interest are shown (Wo, wollastonite; An, anorthite; Mu, mullite; SiO_2, quartz).

particularly K_2O and Na_2O that may cause significant melting/freezing point depressions.

4.5. Thermal analyses

The result of a thermal gravimetric and heat flow analysis of a slightly burnt building earth from the Mureybet site (cf. Fig. 3F) is shown in Fig. 8. The lower graph shows the mass loss in percentage and its derivative as a function of temperature from ambient to 1200 °C. The upper graph shows the corresponding heat flow (mW). The initial endothermic lump below 200 °C is related to drying. Decomposition is initiated at about 450 °C and continues to 725 °C with the breakdown of carbonate. The subsequent large endothermic lump in the heat flux between ~800 and ~1150 °C is attributed to melting, with the later value consistent with the eutectic melting point in the simplified CAS system (Fig. 7). There are further no indications for the presence of organic material that would have appeared as exothermic peaks in the heat flow data at temperatures of 250–450 °C. This is, however, expected since the sample had been observed to have had been burnt and that indications of cereal ash particles are commonly observed associated with building material (Fig. 3F) and many of the scoria droplets (Fig. 3B, H).

4.6. Thermochemical modelling

A simplified thermodynamic model is shown in Fig. 9A based on Gibbs free-energy minimization. The modelling is simplified because it uses an average scoria composition (Table 2) and does not incorporate oxygen in excess of that admitted by the conventional presentation of the chemical analyses. A gas phase does thus not develop and likewise all iron is modelled as ferrous iron as dictated by the model input. Despite such shortcomings, the model provides some basic guidelines for the melting and crystallization of the scoria. The initial melting occurs at about 815–820 °C by melting of phosphate, sodium and potassium silicates, and quartz. The subsequent silicates melting are sodium pyroxene (860 °C), fayalite (975 °C), wollastonite (1025 °C), anorthite (1125 °C), and finally diopside (1175 °C), when the melt composition is similar to the starting composition. The persistence of diopsidic pyroxene and calcic-plagioclase to the near liquidus suggests a two-mineral phase control near the liquidus. This conforms to the implication from the CAS liquidus phase diagram (Fig. 7) that suggests an approach to the eutectic melting point involving quartz in addition to the same two modelled silicate phases. The results are also consistent with the observations from the scoria that silicate melts coexist with Ca-plagioclase and diopsidic pyroxene and that large quartz (or tridymite) grains only record marginal resorption (Fig. 4C). The limited compositional contribution of quartz to the melt can also be observed on the binary oxide-variation diagrams of Fig. 5.

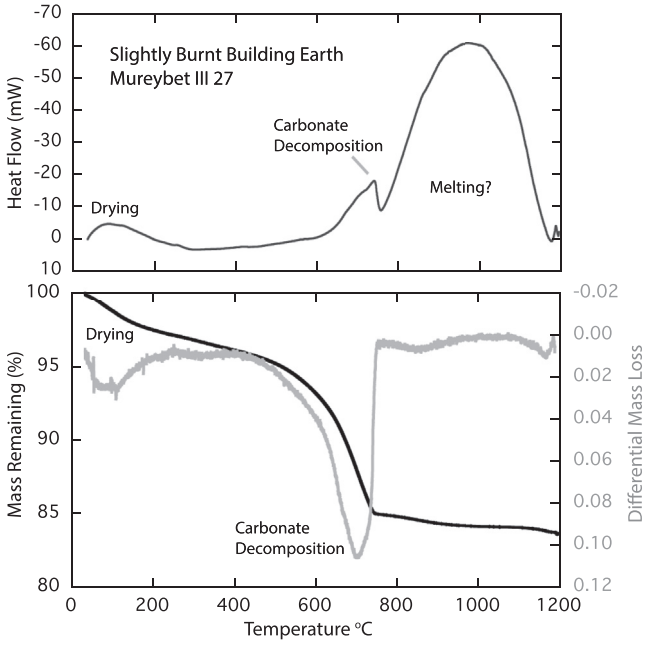

Fig. 8. Thermal gravimetrical and heat flow analysis of building earth from Mureybet from ambiant to 1200 °C. Lower graph is the mass loss in wt. % of the original together with its first derivative. Upper graph shows the corresponding heat flow (mW).

The modelled silicate melt compositions in wt. % are shown in Fig. 9B as a function of temperature. The initial low temperature melt vary widely because of the low melt fraction and the melting of minor phases such as quartz, sodium and potassium silicates, and phosphate. However, from about 1000 °C the melt composition stabilizes with relatively constant compositions of Al_2O_3, SiO_2, Na_2O, and K_2O, decreasing FeO, and increasing CaO and MgO. At 1000 °C nearly 60% (by weight) is melt coexisting with dominating anorthite (Ca-plagioclase) and diopside and minor amount of wollastonite. Using the melt composition analyzed in the scoria droplets (CaO, MgO), it can tentatively be estimated that these record temperatures between 975 and 1175 °C (Fig. 9B).

5. Discussion

5.1. Composition

The major element composition of the scoria droplets and walls shows many similarities to average local and global soils and continental crust compositions (Gromet et al., 1984; Shacklette and Boerngen, 1984; Bradford et al., 1996; Rudnick and Gao, 2003), despite that little site-specific information are available. The northern Syrian soils in the area of interest are the product of arid or semi-arid climate conditions and soil development on a carbonate platform (Brew et al., 2001). This results in the development of cemented horizons of calcite and gypsum and thus a general enrichment of calcium and sulfur in surface soil profiles (Ilaiwi, 2001) and explains the high CaO contents (10–26 wt. %) of the scoria and the surface soil from Abu Hureyra (Bunch et al., 2012). The point analyses of scoria glass in this study (Table 2) and by Bunch et al. (2012) and Wittke et al. (2013) are all substantially above the CaO concentration (2–4 wt. %) in average soil and continental crust estimations (Fig. 5).

Scoria droplets closely resembling the Syrian finds have been described from two North America locations (Bunch et al., 2012; Wittke et al., 2013; Wu et al., 2013) associated with a black mat layer with high organic content (Blackville SC and Melrose PA). This black layer is widely associated with the Younger Dryas interglacial cooling episode about 12,900 years ago (Broecker et al., 2010; Pinter et al., 2011; van Hoesel et al., 2014) and has been found at archeological as well as numerous locations without identified human activity (Haynes, 2007, 2008). Both of these New World locations suggest scoria compositions with low CaO resembling the local soils and thus are compositionally distinct from the Syrian compositions (Fig. 5). These limited observations reinforce the general expectation that the scoria, in common with tektites, is largely controlled by local host soil. However, both the Blackville and the Melrose sites do not record evidence for human activity, suggesting, in contrast to the Syrian sites, that scoria from these may have had a natural origin.

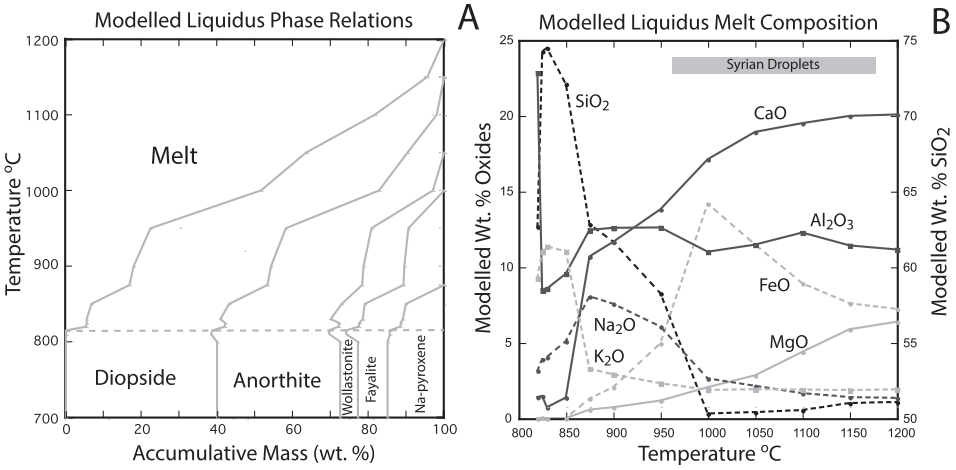

Fig. 9. Thermodynamic modelling of the melting behaviour and melt composition using Gibbs free-energy minimization, the FactSage thermochemical software, and an average glass composition (Table 2). (A) Temperature (°C) as a function of accumulative mass. (B) Modelled melt oxide composition as a function of temperature (°C).

The compositions of tektites illustrated by the Australasian strewn field are compared to the scoria droplets in Fig. 5. The Australasian glassy droplets are attributed to a single low-angle impact about 0.8 Ma ago, probably located in a shallow marine environment of the Gulf of Tonkin, strewing high temperature and pressure melting products (tektite droplets) over a large asymmetric area of the southeastern hemisphere (Koeberl, 1986, 2007; Glass, 1990). Tektites are characterized by widespread deposition, aerodynamically formed shapes, massive glass with few relict and quench minerals (high melting temperature), low vesicle components (low volatile content), overall compositions that reflect the regional source sediments, reduced conditions (low f_{O2}), high pressure mineralogy (coesite, shock deformation), inclusions of SiO_2 glass particles (lechatelierite, resulting from high temperature melting of pure quartz grains), flow and deformation, and possibly high temperature elemental losses. Although the Syrian siliceous droplets show some similarities to tektites (overall shape and records of source rock compositions), they differ on some critical important points. Particularly, the scoria occurs localized and not widespread, is highly vesicular suggesting a high volatile component during melting and cooling, are highly heterogeneous, and furthermore lacks, as discussed below, all clear evidence for high pressure and high temperature processes.

5.2. Textures and mineralogy

The textures of the Syrian scoria show strong evidence for partial melting of a heterogeneous source material, short heating duration, moderate cooling rate, and a general lack of equilibrium melting relations.

The textures are best interpreted as a result of incomplete melting of a heterogeneous building earth composed of fine-grained soil, carbonate, and clay matrix with larger interspersed grains of feldspars (plagioclase and orthoclase) and quartz (low quartz). Melting was initialized and proceeded in the fine-grained matrix at solidus conditions, resulting in melt (or glass) patches at the peak temperature. This interpretation is supported by an X-ray diffraction pattern of burnt building earth that record the same minerals as observed in the partially melted droplets. The composition of these melt patches cluster around the binary anorthite and wollastonite or eutectic melting relations of tridymite, anorthite, and wollastonite, in the ternary CAS system (Fig. 7) (equivalent to quartz, plagioclase, and Ca-pyroxene in the corresponding natural system). The major element variation shown in Fig. 5 suggests that the melt is dominated by melting of Ca-pyroxene and plagioclase and that quartz contributed a smaller proportion to the melting.

This melting mineralogy inferred from ternary system is consistent with the petrographic observations (Fig. 5; Inline Supplementary Table 1) and implies reactions and equilibration with increasing but moderate temperatures as preserved in the less-affected building earth fragments (Fig. 2). The larger feldspar grains and particularly the quartz grains are less affected by melting (Fig. 4), simply because their sizes isolated them from reactions with the fine-grained matrix.

Building earth contains significant quantities of cereal chaff used as a tempering material (Willcox and Fornite, 1999; Willcox and Stordeur, 2012). Cereal chaff and straw were abundant at the dwelling sites and surroundings (wild rye, barley, and wheat). Wood was used for heating and cooking (soft wood like willow and poplar) and wood ash is thus likely to have been present in significant amounts in the source soil. The presence of un-melted, silica-rich plant phytoliths resembling fragments of cereal chaff is clearly revealed in the building earth fragments (Fig. 3F). Silica-rich straw or chaff phytoliths remains can be seen attached to or imbedded in many scoria droplets without sign of melting (Fig. 3B, H). Similar plant tissue can be observed in Fig. 11A of Bunch et al. (2012). This non-reactive nature of the ash fragments is expected considering that straw and chaff ash is composed of either near pure silica or mixtures of potassium and dominating silica with melting well above the minimum melting conditions of the main fine-grained component of the building earth material.

The most conspicuous petrographic feature of the droplets is the strong vesiculation from large bubbles contained by thin walls and minute vesicles imbedded in the walls and more massive parts. The development of a gas phase during heating is controlled by dehydration of hydrous and hydrated minerals (100–300 °C), breakdown of organic material (200–600 °C), and decomposition of carbonates and other minerals (600–800 °C). This gas expansion may have been aided by air draft through the burning building. The initial dehydration may have resulted in fracturing of the building earth, but with increasing temperature, the development of a gas phase could coincide with melting and thus result in foaming and bubbles surrounded by thin silicate melt film (Figs. 3 and 4). The smaller vesicles probably formed during cooling as a result of exsolution of volatiles at high temperature dissolved in the silicate melt.

The formation of a gas phase was aided by cereal remains mixed into the building earth during construction (Fig. 3F). An estimate of about 30% by volume of cereal straw would not appear excessive

and would result in the formation of say ~20 wt. % inorganic ash and a large and strongly temperature dependent gas volume easily amounting at 1000 °C to 20 cubic meters of gas per kg of imbedded organics (calculation based on typical California wheat straw without excess air). This could result in strong fragmentation during decomposition of the organic matter (300–600 °C) and additionally in vesiculation during melting (>700–800 °C) and the formation of scoria droplets.

The mineralogy observed in the Syrian droplets (Inline Supplementary Table 1) is in general consistent with the expectations from the simplified silicate systems (Fig. 7) and melting associated with cotectics in ternary systems. Bunch et al. (2012) described similar scoria droplets as described here from Abu Hureyra. Their Si-rich group of objects is stated as being composed of quartz, plagioclase, and orthoclase, in addition to the silicate melt, and thus is rather similar to the present droplets. They further describe pure-silica fragments showing sigh of viscous flow and interpreted these as having resulted from ultra-high temperature, shock-melting of quartz minerals (lechatelierite) as elsewhere documented from known impact, lightning, and detonation sites (see also Wittke et al., 2013). Such pure-silica glass was not detected in the present study where the maximum silica content was <55 wt. SiO_2; however we note that the presence of flow lines in viscous silicate melts is an expectation particularly in aerodynamically shaped scoria and pyroclastic pumice (Heiken and Wohletz, 1985) and furthermore an apparent intrinsic characteristic of many nearly pure-silica ash fragments of straw materials (Fig. 3B, H). Wittke et al. (2013) further observed marginal depletion in the content of SiO_2 for some droplets and related this to high pressure and high temperature volatilization or boiling, while for other droplets, with increase in SiO_2 toward the margins, they advocated condensation. Such observations together with inferred very high temperature (>2200 °C) based on the mineralogy (mainly quartz minerals) was used to support cosmic airburst or impact as the origin of the scoria droplets.

Scoria droplets have been described from two additional North American Younger Dryas locations, one in Pennsylvania (Melrose) and one in South Carolina (Blackville). The droplets from Melrose (Wu et al., 2013) differ in composition from the Syrian droplets with much smaller calcium concentrations thus more like typical average soils and continental crust. Their mineralogy includes mullite, corundum, cordierite, quartz, and magnetite. This is consistent with their near binary composition in the CAS system (Fig. 7) as well as the more appropriate $FeO{\cdot}Fe_2O_3$–Al_2O_3–SiO_2 (FAS) system, where they plot in the mullite field, bordering to corundum and quartz (Fig. 10).

The results of subsurface burning of coal seams (Stracher, 2007) are often described as clinker, scoria, and (para) lava attributed to low-pressure formation temperatures of 1000–1400 °C (Cosca et al., 1989; Vapnik et al., 2007; Masalehdani et al., 2007). The products of such combustion metamorphism show many similarities to those found in the Melrose droplets, including partial melting and mineral assemblages with mullite.

In addition to the silicate minerals, Wu et al. (2013) reported Fe-rich minerals (native iron, magnetite, sulfide, suessite) (~Fe_3C), and schreibersite (~Fe_3P)) from the Melrose location that may indicate reduced conditions (low-f_{O2}) for three droplets or about 15% of the reported analyses. Interaction between organic material in the form of coal-rich beds and basaltic lava are known to cause reduced

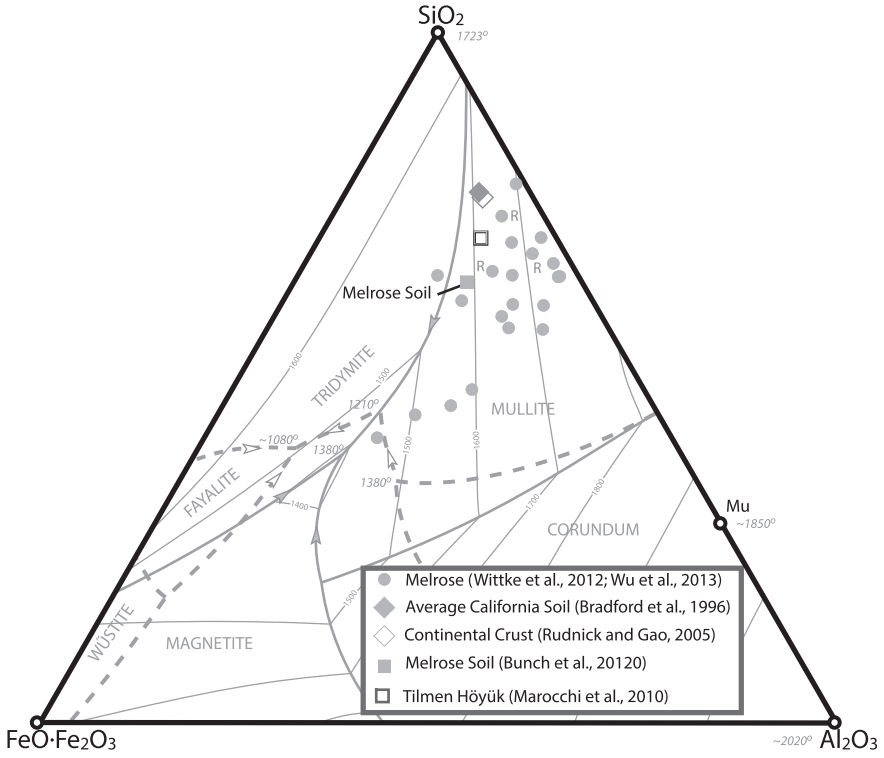

Fig. 10. Part of the simplified liquidus surface in the Fe_2O_3–FeO–Al_2O_3–SiO_2 quaternary diagram projected on the Fe_2O_3. FeO–Al_2O_3–SiO_2 triangular diagram. Projections are shown for oxidized (full drawn phase boundaries) and reduced conditions (stippled) both constructed from Muan (1957). The liquidus surface is for oxidized conditions contoured for temperature. The univariant lines with arrows indicate decreasing temperature and the eutectic points are shown with temperatures in italic. The data plotted is the Melrose compositions (Wittke et al., 2013; Wu et al., 2013); local Melrose soil compositions by Bunch et al. (2012); average California soil from Bradford et al. (1996); and continental crust from Rudnick and Gao (2003). Tilmen Höyük is a basaltic glass in vitrified building block from Marocchi et al. (2010). The Melrose scoria compositions marked 'R' were identified as reduced by Wu et al. (2013).

mineralogy, including, in addition to troilite (FeS), the same phases as observed for the Melrose droplets, and interpreted to have formed at atmospheric pressures and temperatures below 1250 °C (Pedersen, 1979a,b; 1985). The oxygen pressure (or oxidation) may thus vary dependent on the amount of organic material in the source and may affect the major as well as mineralogy and melting relations. The observations from the Syrian droplets suggest that the main part of iron is oxidized to Fe_2O_3 and thus question the use of the relatively reduced FeO–Al_2O_3–SiO_2 simplified system, as done by Bunch et al. (2012) and Wu et al. (2013), when ternary projections of the quaternary FeO–Fe_2O_3–Al_2O_3–SiO_2 may be more appropriate for the redox conditions prevailing during formation of the droplets (Fig. 10).

5.3. Estimates of melting temperature

When estimating melting temperatures using compositional data, as done in this study, as well as by Wu et al. (2013), it is essential to understand what the data represent. The point analyses obtained in this study with the EMP represent the melt (now quenched as a glass) present in the droplets. The alternative would be to analyze a larger area also with the EMP in order to obtain analyses that represent the bulk compositions of the droplets. The former approach would ideally allow us to trace the initial melting process and to estimate the melting temperature. The latter approach would ideally allow an estimate of the final fictitious equilibrium temperature when all minerals have melted and only melt remains. This latter was apparently chosen by Bunch et al. (2012) and Wittke et al. (2013), although the descriptions of their analytical methods are not conclusive. For materials that represent non-equilibrium and incomplete melting, as argued here, this approach may be fatal for obtaining reliable temperature estimates.

The melts in the Syrian droplets projects around binary melting relations approaching eutectic melting in the CAS ternary system indicating temperatures of 1170 °C, or above (Fig. 7). The results by Bunch et al. (2012) and Wittke et al. (2013) varies from the same eutectic towards the SiO_2 apex, suggesting an increasing component of un-melted quartz incorporated into the analyses. These analyses thus do not necessary imply increased melting temperature to 1500 °C, or above, as directly read from the phase diagram (Fig. 7). The trend toward increasing SiO_2 is further inconsistent with the Abu Hureyra soil analyzed by Bunch et al. (2012). Increasing melting of that soil may be predicted to move toward the soil composition away from SiO_2 and the 1170 °C eutectic to a liquidus at about 1300 °C, within the wollastonite field; although it should in fairness be pointed out that the soil composition plots just outside the Wo-Q-An triangle and strictly interpreted should form initial melts at the 1265 °C eutectic, saturated in gehlenite instead of quartz (Fig. 7).

Supporting evidence for a low initial melting is offered by the thermal analyses of a sample of a burnt building earth, representing typical source material (Fig. 8). The results represent equilibrium melting (because the sample was ground to a fine powder) and not the disequilibrium melting suggested by the petrography of the droplets. Following initial drying of the sample to 200 °C and carbonate decomposition at ~700 °C, an area is encountered with steady endothermic increase in the heat flow without mass loss until a maximum of ~1000 °C, after which the heat flow decreases markedly to 1200 °C. This variation is interpreted as reflecting initial melting at just after 700 °C and termination of melting at about 1200 °C. Thermochemical modelling based on an average melt composition supports in general such low initial temperatures (~825 °C) and total melting at 1200 °C (Fig. 9A), although the predicted mineralogy assemblage do not entirely duplicate the petrographic observations suggesting that quartz is completely eliminated at the eutectic and have little effects on the subsequent subliquidus melt compositions (Fig. 9B). This latter is also suggested by the compositional variability of the analyzed glasses (Fig. 5).

The Melrose (and Blackwille) droplets are not well represented by the CAS simplified system because of their low CaO content and the possibility for variable oxygen pressure (Wu et al., 2013). The compositions of the Melrose droplets are therefore projected onto ternaries of the quaternary FeO–Fe_2O_3–Al_2O_3–SiO_2 (Fig. 10). The droplets project, together with the various soils and continental crust, within the mullite field on the FeO·Fe_2O_3–Al_2O_3–SiO_2 ternary; suggesting very high liquidus temperatures of 1550–1750 °C for equilibrium melting of the bulk droplets. The group of glass analyses by Wu et al. (2013) fans out from the general field toward the piercing eutectic at 1380 °C for oxidized conditions or 1080 °C for reduced conditions (Fig. 10).

The use of ternary liquidus surface diagrams is fraught with uncertainty since must natural systems are of a multi-component nature, often including ten different oxides. The most important components, not included in the diagrams discussed, are Na_2O and K_2O of which only small amounts will greatly lower the liquidus surfaces and thus the temperature estimates (Fig. 11). In the R_2O–Al_2O_3–SiO_2 systems (where R is Na or K), the effect of the addition of 25% K_2O or Na_2O (or both) will drop the liquidus to a cotectic temperature of 710–985 °C for K_2O or to 1050–740 °C for Na_2O, saturated in mullite. Initial melting in the multi-component silicate systems of which the droplets are composed may thus initiate at very low temperatures and may with increasing temperature proceed to very high degree of melting of the whole of the source. As demonstrated for the Syrian droplets, these reflect incomplete and disequilibrium melting and can thus not have reached temperatures as high as suggested from their bulk compositions by Bunch et al. (2012) and Wittke et al. (2013). The maximum temperature for the Syrian droplets is suggested by the thermal analyses and modelling to be in the range of 1000–1200 °C (Figs. 8 and 9).

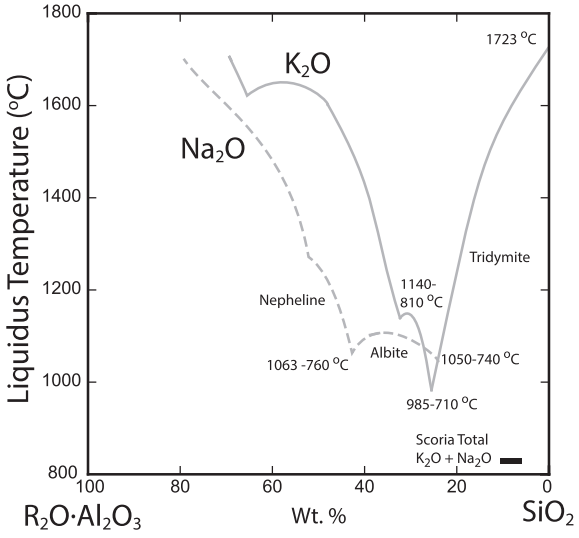

Fig. 11. Traces of liquidus surfaces in the K_2O–Al_2O_3–SiO_2 and Na_2O–Al_2O_3–SiO_2 (Levin et al., 1964; Muan and Osborn, 1965) systems projected on temperature (°C) against the binary SiO_2–$R_2O.Al_2O_3$, where R is either K or Na. Temperatures are the melting temperatures on the piercing cotectics. Range in total K_2O + Na_2O for the scoria droplets (Wittke et al., 2013; Wu et al., 2013) are given in the lower right corner suggesting complete melting at temperatures of 1550–1625 °C.

5.4. Fingerprinting using trace elements

The trace element concentration of the droplets reflects the components making up the source. The building earth at the Syrian sites is likely composed of the local soil, including cultural additions such as wood ash dispersed from the hearths of the dwellings and cereal straws and other organic waste. The former is reflected in the abundance of charcoal and ash in the archaeological soil. The latter is abundantly observed in the earth material of the buildings and also from the partially melted droplets. The background soil of the Syrian sites, however, is not known in any detail, but judging from a general knowledge of the regional soil types it is reasonable to expect a heterogeneous mixture of clays, quartz, feldspars, and carbonates. The presence of carbonate is detected by the thermal analysis where this phase breaks down between 600 and 700 °C (Fig. 8), while large quartz and feldspar grains can still be observed as relict grains in all the scoria droplets. The local chalk was used as part of the building material at Jerf el Ahmar, Dja'de, Murerybet, and Qaramel. Chalk blocks were used in the walls and floors. Some grinding stones and other tools were made of limestone. The large CaO content of both the local soil (Bunch et al., 2012) and the droplet compositions suggests that carbonate was an inherent component of the site soil. Large amount of carbonate was detected by both the thermal analyses (Fig. 8) and also by X-ray diffraction (where quartz and calcite dominate). It can thus be expected that the trace element concentrations will record the original soil, including carbonate, and organic materials, mainly straw and wood ashes. As already pointed out, an extraterrestrial or impact component, using the platinum-group elements, could not be detected.

The trace element concentrations are shown in Fig. 6 normalized to an average global crust composition (Rudnick and Gao, 2003), serving as a proxy for the local Syrian soil. Deviations from the horizontal stippled line (=1) reflect either the local soil and/or components added to the soil to produce the building earth. With an estimated 30% straw component by volume in the building earth subjected to increasing temperature, a fair amount of ash (~10–20 % by weight) will be left, composed of large flakes of inorganic components and some charcoal dependent on the availability of oxygen during decomposition. This ash will be largely isolated from reacting with the finer fractions of the earth material and will thus contribute marginally to the droplet compositions. Furthermore, the main components in wheat and grass ash will be silica and potassium and will contain few, if any, major and trace elements concentrations above continental curst and soil compositions (Thy et al., 2013a,b). On the other hand, ash of soft wood materials, like willow, poplar, and fir, may display significant elemental enrichments compared to continental crust, particularly in calcium (Ca), strontium (Sr < 1700 ppm), and cadmium (Cd < 70 ppm) (Thy et al., 2013a,b; Phyllis2 Database, 2014). These elements are enriched in the Syrian droplets (Figs. 5 and 6, Inline Supplementary Table 2), with notable values for Cd reaching about 10 times enrichment compared to continental crust (or an absolute average of ~1 ppm) and for Sr about 5 times (or an absolute average of 670 ppm). Thus even a small amount of wood ash mixed into the soil would result in significant enrichments in the droplet concentrations, particularly for Cd. Wood ash is very fine and would easy be mixed into surface soil at active settlement sites and would thus be accessible for melting, much more so than straw ash. It is, however, possible that the high content of carbonate in the earth material can be the carrier of Sr and Cd. Sedimentary and deep-sea carbonate rocks typically contain high amounts of Sr (600–1000 ppm), but small amounts of Cd (0.04–0.07) (Turekian and Wedepohl, 1961; Veizer, 1983). Thus particularly the Cd contents of the droplets may be affected by wood ash, although the wood ash content appears to be highly variable, because of levels below detection limit for Cd in two of the droplets analyzed (Inline Supplementary Table 2).

5.5. Shapes and formation

The shapes of the observed scoria particle are diagnostic for aerodynamically rotating fluid droplets by showing symmetrical elongation along a dominating axis of rotation and depending on surface energy and viscosity eventual splitting into dumbbell and teardrop shapes. In these aspects they show similarities to tektites (Butler et al., 2011).

Two modern-day industrial products, however, provide better comparisons. The first of these are spherules commonly found in ash from coal and biomass fired power plants normally referred to as cenospheres (Fenelonov et al., 2010; Li et al., 2013a,b; Joseph et al., 2013). The characteristics of cenospheres depends on the fuel source, but are commonly described as hollow spheres with a thin wall composed of amorphous aluminosilicate glass and/or quartz and mullite. Cenospheres range form having near perfect spherical shapes with diameters between 20 and 200 μm and a rather constant wall thickness (2–10 μm) to larger (<0.5 mm) irregular spherules with an internal network of walls and bobbles (Li, 2012). The latter is similar to droplets discussed in this study. Their compositions (Li, 2012) are mainly made up of SiO_2 (55–70 wt. %), Al_2O_3 (25–45 wt. %) and Fe_2O_3 (<10%) and thus compares to the scoria droplets from the Melrose location. Sintering temperatures are estimated to start at 1000–1200 °C and melting to be completed at 1300–1400 °C (Raask, 1968; Vassilev et al., 2004), again rather similar to the finding for the Melrose droplets, although Li et al. (2013b) suggested fluid temperatures to well above 1650 °C for cenospheres in coal fired boilers.

The other industrial product of interest in this context is light expanded clay aggregates (LECA) widely used in building materials and many other applications. The production of LECA particles involves the injection of a watery sludge of clay, organics, and carbonates into a rotary electric kiln held at temperatures of 1100–1200 °C (Bogas et al., 2012). The resultant product is irregular to spherical particles (<30 mm) composed of an outer glassy wall (~200 μm thick) and an inner foamed fabric of honeycomb voids and glassy walls. Again, these are similar to the siliceous scoria as far as shape and internal fabric is concerned. Despite that the detailed recipes for LECA may vary widely and are often confidential, the general makeup of the reactant appears to contain the same basic ingredients suggested for the Syrian droplets. Characterizing the formation of the boiler and the LECA particles, as well as the Syrian droplets, is an expanding gas phase in a high temperature environment and the presence of viscous aluminosilicate melts.

5.6. Younger Dryas Impact Hypotheses

A Younger Dryas impact in North America was originally advocated by Firestone et al. (2006, 2007) to explain various observations, several of which originated from particles found in black mat deposits in North America, Europe, and the Middle East, all dated to around 12,900 years ago (or the start of the Younger Dryas). Several types of particles were reported and related to melting at elevated temperature resulting from cosmic impact. The idea has received widespread attention and discussion still continues without an emergent general consensus (e.g. Surovell et al., 2009; Kennett et al., 2009; Haynes et al., 2010; French and Koeberl, 2010: Kerr, 2010; Pinter et al., 2011; LaCompte et al., 2012; Bunch et al., 2012; Wittke et al., 2013; van Hoesel et al., 2014; Wu et al., 2013). Boslough et al. (2012) synthesized a large number of critical problems with the Younger Dryas Impact Event hypothesis, including reporting radiocarbon dates on carbonaceous spherules

from North America that do not fit with a Younger Dryas age (cf. Meltzer et al., 2014). However, there has not previously been a geochemical assessment on the composition and formation of the siliceous spherules, as provided by the present study.

Of interest to the present discussion is that recent studies by Bunch et al. (2012), Wittke et al. (2013), and Wu et al. (2013) have described finds of siliceous scoria droplets attributed to very high temperature melting of the target soil by a cosmic Younger Dryas impact. Wittke et al. (2013) has advocated that ten million tons of impact spherules were spread across four continents, including the Syrian sites, resulting from a Younger Dryas impact in an ice sheet in North America. We have here clearly demonstrated that particles from such a strewn field are not represented at the sites in Syria, simply because of conflict between site ages and estimated low melting temperatures of the droplets studied.

6. Conclusions

Siliceous scoria droplets are found in association with several early agricultural settlements along the Euphrates River in northern Syria. The radiocarbon dates of the sites and excavation levels range from 13,200 to 10,200 years ago, thus are unrelated to the onset of the global Younger Dryas cooling event at around 12,900 years ago. The majority of the locations include mudbrick building structures, which in some cases show sign of intense fire and surface melting. The appearance of scoria is rare and localized without being widespread as would have been implied by the nearly worldwide impact strewn field theory.

The main source of the scoria droplets is the local soils identified by high calcium content. It is concluded that building earth made from a mixture of the local soil and cereal straw partially melted during firestorms through dwellings. The peak temperature (<1200 °C) was short-lived resulting in strong disequilibrium partial melting. Strong air draft through the structure together with dehydration and decomposition processes of organics and carbonate aided the melting and resulted in aerodynamically shaped partial melted particles sprawled from the melting site.

There is in the present study no support for scoria fall-out from a distant impact source at the Syrian archaeological sites. Our results, however, do not necessarily discredit the Younger Dryas Impact hypothesis, although we caution about relying uncritically on findings from similar particles from other sites and locations.

Acknowledgements

The Electron Microprobe Laboratory of the Department of Earth and Planetary Science, University of California at Davis, was used for the quantitative analyses and imaging. The NEAT Thermochemistry Facility, University of California at Davis, provided access to the FactSage software and databases. The LA-ICPMS analyses were done at the UC Davis Interdisciplinary Center for Plasma Mass Spectrometry. We are grateful for the help and comments provided by O. Stecher (tektites), B.M. Jenkins (biomass boilers), J.C. Fettinger (XRD), as well as official and unofficial reviewers. C.E. Lesher is thanked for his constant encouragements and support. A Niels Bohr Professorship funded by Danish National Research Foundation to Aarhus University, Denmark in part supported this research.

References

Baker, G., 1968. Micro-forms of hay-silica glass and of volcanic glass. Mineral. Mag. 36, 1012–1023.
Baker, G., Gaskin, A.J., 1946. Natural glass from Macedon, Victoria, and its relationships to other natural glasses. J. Geol. 54, 88–104.
Bale, C.W., Chartrand, P., Degterov, S.A., Eriksson, G., Hack, K., Mahfoud, R.B., Melançon, J., Pelton, A.D., Petersen, S., 2002. FactSage thermochemical software and database. Calphad 26, 189–228.
Bogas, J.A., Mauricio, A., Pereira, M.F.C., 2012. Microstructural analyses of Iberian expanded clay aggregates. Microsc. Microanal. 18, 1190–1208.
Boslough, M., Nicoll, K., Holliday, V., Daulton, T.L., Meltzer, D., Pinter, N., Scott, A.C., Surovell, T., Claeys, P., Gill, J., Paquay, F., Marlon, J., Bartlein, P., Whitlock, W., Grayson, D., Jull, A.J.T., 2012. Arguments and evidence against a Younger Dryas impact event. In: Goisan, L., Fuller, D.Q., Nicoll, K., Flad, R.K., Clift, P.D. (Eds.), Climates, Landscapes, and Civilizations. American Geophysical Union, Washington, DC, pp. 13–26.
Bradford, G.R., Chang, A.C., Page, A.L., Bakhtar, D., Frampton, J.A., Wright, H., 1996. Background Concentrations of Trace and Major Elements in California Soils. Kearney Foundation of Soil Science, Division of Agriculture and Natural Resources, University of California, pp. 1–32.
Braemer, F., Echallier, J-Cl, Taraqji, A., 2004. Khirbet al Umbashi: villages et campements de pasteurs dans le désert noir (Syrie) à l'âge du Bronze. Bibliothèque archéologique et historique tombe 171. Institut français du Proche-Orient, Beyrouth.
Brew, G., Barazangi, M., Al-Maleh, A.K., Sawaf, T., 2001. Tectonic and geologic evolution of Syria. GeoArabia 6 (4), 573–615. GulfPetroLink, Bahrain.
Broecker, W.S., Denton, G.H., Edwards, R.L., Cheng, H., Alley, R.B., Putnam, A.E., 2010. Putting the Younger Dryas cold event into context. Quat. Sci. Rev. 29, 1078–1081.
Brothwell, D.R., Bishop, A.C., Woolley, A.R., 1974. Vitrified forts in Scotland: a problem in interpretation and primitive technology. J. Archaeol. Sci. 1, 101–107.
Bryan, J.L., 1980. Building fires. J. Archit. Educ. 33, 32–37.
Bryant, G.W., Browning, G.J., Emanuel, H., Gupta, S.K., Gupta, R.P., Lucas, J.A., Wall, T.F., 2000. The fusibility of blended coal ash. Energy Fuels 14, 316–325.
Bunch, T.E., Hermes, R.E., Moore, A.M.T., Kennett, D.J., Weaver, J.C., Wittke, J.H., DeCarli, P.S., Bischoff, J.L., Hillman, G.C., Howard, G.A., Kimbel, D.R., Kletetschka, G., Lipo, C.P., Sakai, S., Revay, Z., West, A., Firestone, R.B., Kennett, J.P., 2012. Very high-temperature impact melt products as evidence for cosmic airbursts and impacts 12,900 years ago. Proc. Natl. Acad. Sci. 109, E1903–E1912.
Butler, S.L., Stauffer, M.R., Sinha, G., Lilly, A., Spiteri, R.J., 2011. The shape distribution of splash-form tectites predicted by numerical simulation of rotating fluid drops. J. Fluid Mech. 667, 358–368.
Cashman, K.V., Mangan, M.T., 1994. Physical aspects of magmatic degassing II: constraints on vesiculation processes from textural studies of eruptive products. In: Carroll, M., Holloway, J.R. (Eds.), Volatiles in Magmas. Reviews of Mineralogy, vol. 30. Mineralogical Society of America, Washington, D.C, pp. 447–478.
Çatalhöyük Archive Reports, http://www.catalhoyuk.com/downloads/Archive_Report_2005.pdf page 238 and http://www.catalhoyuk.com/downloads/Archive_Report_2011.pdf page 31 (accessed June 2014).
Childe, V.G., Thorneycroft, W., 1937. The experimental production of the phenomena distinctive of vitrified forts. Proc. Soc. Antiq. Scotl. 72, 44–55.
Colledge, S., Conolly, J., 2010. Reassessing the evidence for the cultivation of wild crops during the Younger Dryas at Tell Abu Hureyra, Syria. Environ. Archaeol. 15, 124–138.
Coqueugniot, É., 2000. Dja'de (Syrie), un village à la veille de la domestication (seconde moitié du 9e millénaire av. J.C.). In: Guilaine, J. (Ed.), Les premiers paysans du monde, naissance des agricultures. Errance, Paris, pp. 63–79.
Cosca, M.A., Essene, E.J., Geissman, J.W., Simmons, W.B., Coates, D.A., 1989. Pyrometamorphic rocks associated with naturally burned coal beds, Powder River Basin, Wyoming. Am. Mineral. 74, 85–100.
Denbow, J., Smith, J., Ndobochani, N.M., Atwood, K., Miller, D., 2008. Archaeological excavations at Bosutswe, Botswana: cultural chronology, paleo-ecology and economy. J. Archaeol. Sci. 35, 459–480.
Evans, N.J., Gregoire, D.C., Grieve, R.A.F., Goodfellow, W.D., Veizer, J., 1993. Use of platinum-group elements for impact identification: terrestrial impact craters and Cretaceious-Tertiary boundary. Geochim. Cosmochim. Acta 57, 3737–3748.
Fenelonov, V.B., Mel'gunov, M.S., Parmon, V.N., 2010. The properties of cenospheres and the mechanism of their formation during high-temperature coal combustion at thermal power plants. KONA Power Part. J. 28, 189–208.
Firestone, R.B., West, A., Warwick-Smith, S., 2006. The Cycle of Cosmic Catastrophes. Bear & Company, Rochester, Vermont.
Firestone, R.B., West, A., Kennett, J.P., Becker, L., Bunch, T.E., Revay, Z.S., Schultz, P.H., Belgya, T., Kennett, D.J., Erlandson, J.M., Dickenson, O.J., Goodyear, A.C., Harris, R.S., Howard, G.A., Kloosterman, J.B., Lechler, P., Mayewskio, P.A., Montgomery, J., Poreda, R., Darrah, T., Que Hee, S.S., Smith, A.R., Stich, A., Topping, W., Wittke, J.H., Wolbach, W.S., 2007. Evidence for an extraterrestrial impact 12,900 years ago that contributed to the megafaunal extinctions and the Younger Dryas cooling. Proc. Natl. Acad. Sci. 1104, 16016–16021.
Fleischmann, C.M., Parkes, A.R., 1997. Effects of ventilation on the compartment enhanced mass loss rate. In: Hasemi, Y. (Ed.), Fire Safety Science-proceedings of the Fifth International Symposium, pp. 415–426.
Folk, R.L., Hoops, G.K., 1982. An early iron-age layer of glass made from plants at Tel Yin'am. Israel J. Field Archaeol. 9, 455–466.
French, B.M., Koeberl, C., 2010. The convincing identification of terrestrial meteorite impact structures: what works, what doesn't, and why. Earth Sci. Rev. 98, 123–170.
Friend, C.R.L., Dye, J., Fowler, M.B., 2007. New field and geochemical evidence from vitrified forts in South Morar and Moidart, NW Scotland: further insight into melting and the process of vitrification. J. Archaeol. Sci. 34, 1685–1701.

Friend, C.R.L., Charnley, N.R., Clyne, H., Dye, J., 2008. Experimental produced glass compared with that occurring at the Torr, NW Scotland, UK: vitrification through biotite melting. J. Archaeol. Sci. 35, 3130–3143.
Glass, B.P., 1990. Tektites and microtektites: key facts and inferences. Tectonophysics 171, 393–404.
Gray, V.R., 1987. Prediction of ash fusion temperature from ash composition for some New Zealand coals. Fuel 66, 1230–1239.
Gromet, L.P., Dymek, R.F., Haskin, L.A., Korotev, R.L., 1984. The "North American shale composite": its compilation, major and trace element characteristics. Geochim. Cosmochim. 48, 2469–2482.
Gustavsson, N., Bølviken, B., Smith, D.B., Severson, R.C., 2001. Geochemical Landscapes of the Conterminous United States – New Map Presentations for 22 Elements. U.S. Geological Survey Professional Paper 1648, Denver CO.
Haynes Jr., C.V., 2007. Younger Dryan "black mats" and the Rancholabrean termination in North America. Proc. Natl. Acad. Sci. 105, 6520–6525.
Haynes Jr., C.V., 2008. Nature and origin of the black mat, stratum F_2. In: Haynes, C.V., Huckell, B.B. (Eds.), Murray Springs. A Clovis Site with Multiple Activity Areas in the San Pedro Valley, Arizona. University of Arizona Press, Tucson, pp. 240–249.
Haynes Jr., C.V., Boerner, J., Domanik, K., Lauretta, D., Ballenger, J., Goreva, J., 2010. The Murray Springs Clovis site, Pleistocene extinction, and the question of extraterrestrial impact. Proc. Natl. Acad. Sci. 107, 4010–4015.
Heiken, G., Wohletz, K., 1985. Volcanic Ash. University of California Press, Berkeley.
Henderson, J., Janaway, R., Richards, J., 1987. A curious clinker. J. Archaeol. Sci. 14, 353–365.
Hillman, G.C., Hedges, R., Moore, A., Colledge, S., Pettitt, P., 2001. New evidence of late glacial cereal cultivation at Abu Hureyra on the Euphrates. Holocene 11, 383–393.
Huggins, F.E., Kosmack, D.A., Huffman, G.P., 1981. Correlation between ash-fusion temperature and ternary equilibrium phase diagrams. Fuel 60, 577–584.
Humphreys, S., Shakesby, R.A., Doerr, S.H., Blake, W.H., Wallbrink, P., Hart, D.M., 2003. Some effects of fire on the regolith. In: Roach, I.C. (Ed.), Advances in Regolith. CRC LEME, pp. 216–220.
Ibañez, J. (Ed.), 2008. Le site néolithique de Tell Mureybet (Syrie du Nord), en hommage à Jacques Cauvin. BAR International Series, vol. 1843(1).
Ilaiwi, M., 2001. Soils of the Syrian Arab Republic. In: Zdruli, P., Steduto, P., Lacirignola, C., Montanarella, L. (Eds.), Soil Resources of Southern and Eastern Mediterranean Countries. CIHEAM, Bari, pp. 227–242. Options Méditerranéennes: Série B. Etudes et Recherches; no. 34. http://om.ciheam.org/om/pdf/b34/01002096.pdf (accessed May 24, 2014).
Jak, E., 2002. Prediction of coal ash fusion temperatures with the F*A*C*T thermodynamic computer package. Fuel 81, 1655–1668.
Jacobson, L., Loock, J.C., van der Westhuizen, Huffman, T.N., Dryer, J.J.B., 2003. The occurrence of vitrified dung from the Kamdeboo district, southern Karoo, and Den Staat, Limpopo Valley, South Africa. South Afr. J. Sci. 99, 26–28.
Johansen, G.P., 2004. Landscape, monumental architecture and ritual: a reconsideration of the South Indian Ashmounds. J. Anthropol. Archaeol. 23, 309–330.
Joseph, K.V., Francis, F., Chacko, J., Das, P., Hebbar, G., 2013. Fly ash cenosphere waste formation in coal fired power plants and its application as a structural material – a review. Int. J. Eng. Res. Technol. 2, 1236–1260.
Kalmanovitch, D.P., Williamson, J., 1986. Crystallization of coal ash melts. In: Vorres, K.S. (Ed.), Mineral Matter and Ash in Coal, ACS Symposium Series 301. American Chemical Society, Washington DC, pp. 234–255.
Kennett, D.J., Kennett, J.P., West, A., West, C.J., Bunch, T.E., et al., 2009. Shock-synthesized hexagonal diamonds in Younger Dryas boundary sediments. Proc. Natl. Acad. Sci. 106, 12623–12638.
Kerr, R.A., 2010. Mammoth-killer impact flunks out. Science 329, 1140–1141.
Kilinc, A., Carmichael, I.S.E., Rivers, M.L., Sack, R.O., 1983. The ferric-ferrous ratio of natural silicate liquids equilibrated in air. Contrib. Petrol. Mineral. 83, 136–140.
Klopovic, S., Turan, Ö.F., 2001. A comprehensive study of externally venting flames Part II: plume envelope and centre-line temperature comparisons, secondary fires, wind effects and smoke management system. Fire Saf. J. 36, 135–172.
Koeberl, C., 1986. Geochemistry of tektites and impact glasses. Annu. Rev. Earth Planet. Sci. 14, 323–350.
Koeberl, C., 2007. The geochemistry and cosmochemistry of impacts. Treatise Geochem. 1, 1–52 (Elsevier).
Korisettar, R., Venkatasubbaiah, P.C., Fuller, D.Q., 2001. Brahmagiri and beyond: the archaeology of the southern Neolithic. In: Settar, S., Korisettar, R. (Eds.), Indian Archaeology in Retrospect. Prehistory, vol. 1. Manohar, New Dehli, pp. 151–238.
Kresten, P., Ambrosiani, B., 1992. Swedish vitrified forts – a reconnaissance study. Fornvännen 87, 1–17.
LaCompte, M.A., Goodyear, A.C., Demitroff, M.N., Batchelor, D., Vogel, E.K., Mooney, C., Rock, B.N., Seidel, A.W., 2012. Independent evaluation of conflicting microspherules results from different investigations of the Younger Dryas impact hypothesis. Proc. Natl. Acad. Sci. 109, E2960–E2969.
Levin, E.M., Robbins, C.R., McMurdie, H.F., 1964. Phase Diagrams for Ceramists. American Ceramic Society, Ohio.
Li, Y., 2012. Ash Cenosphere Formation, Fragmentation and its Contribution to Particulate Matter Emission during Solid Fuels Contribution (PhD. thesis). Curtin University, Australia.
Li, Y., Gao, X., Wu, H., 2013a. Further investigation into the formation mechanism of ash cenospheres from an Australian coal-fired power station. Energy Fuels 27, 811–815.
Li, Y., Gao, X., Wu, H., 2013b. Ash cenosphere from solid fuels combustion. Part 2: significant role of ash cenosphere fragmentation in ash and particulate matter formation. Energy Fuels 822–829.
Marocchi, M., Bargossi, G.M., Gasparotto, G., Dondi, M., 2010. Vitrification of basalt orthostats and mud building components from Tilmen Höyuük (south-eastern Turkey): an experimental and eoarchaeological approach. J. Archaeol. Sci. 37, 488–498.
Masalehdani, M.N.-N., Black, P.M., Kobe, H.W., 2007. Mineralogy and petrography of iron-rich slags and paralavas formed by spontaneous coal combustion, Rotowaro coalfield, North Island, New Zealand. In: Stracher, G.B. (Ed.), Geology of Coal Fires: Case Studies from Around the World. Reviews in Engineering Geology, vol. 18. Geological Society of America, pp. 117–131.
Mazurowski, R.F., Kanjou, Y. (Eds.), 2013. Tell Qaramel 1999–2007. Protoneolithic and Early Pre-pottery Neolithic Settlement in Northern Syria. Polish Centre for Mediterranean Archaeology University of Warsaw.
Meltzer, D.J., Holliday, V.T., Cannon, M.D., Miller, D.S., 2014. Chronological evidence fails to support claim of an isochronous widespread layer of cosmic impact indicators dated to 12,800 years ago. Proc. Natl. Acad. Sci. 111, E2163–E2171.
Moore, A., Hillman, G., Legge, T. (Eds.), 2000. Village on the Euphrates, from Foraging to Farming at Abu Hureyra. Oxford University Press, New York.
Muan, A., 1957. Phase equilibria at liquidus temperatures in the system iron oxide-Al_2O_3-SiO_2 in air atmosphere. J. Am. Ceram. Soc. 40, 121–133.
Muan, A., Osborn, E.F., 1965. Phase Equilibria Among Oxides in Steelmaking. American Iron and Steel Institute. Addison-Wesley, Massachusetts.
Pedersen, A.K., 1979a. A shale buchite xenolith with Al-armalcolite and native iron in a lava drom Asuk, Disko, Central West Greenland. Contrib. Mineral. Petrol. 69, 83–94.
Pedersen, A.K., 1979b. Basaltic glass with high-temperature equilibrated immiscible sulphide bodies with natavie iron from Disko, Central West Greenland. Contrib. Mineral. Petrol. 69, 397–407.
Pedersen, A.K., 1985. Reaction between picrite magma and continental crust: early Tertiary silicic basalts and magnesian andesites deom Disko, West Greenland. Bull. Grønl. Geol. Unders. 152, 126 pp.
Phyllis2 Database, 2014. Database for Biomass and Waste. Energy Research Centre of the Netherlands. https://www.ecn.nl/phyllis2/ (accessed June 2014).
Pinter, N., Scott, A.C., Daulton, T.L., Podoll, A., Koeberl, C., Anderson, R.S., Ishman, S.E., 2011. The Younger Dryas impact hypothesis: a requiem. Earth Sci. Rev. 106, 247–264.
Raask, E., 1968. Cenospheres in pulverized-fuel ash. J. Inst. Fuel 43, 339–344.
Rehren, T., 2000. Rationales in Old World base glass compositions. J. Archaeol. Sci. 27, 1225–1234.
Rowe, M.C., Thornber, C.R., Gooding, D.J., Pallister, J.S., 2008. Catalog of Mount St. Helens 2004-2005 Tephra Samples with Major and Trace Element Geochemistry. Open File Report 2008-1131. U.S. Geological Survey.
Rudnick, R.L., Gao, S., 2003. Composition of the continental crust. Treatise Geochem. 3, 1–64 (Elsevier).
Schairer, J.F., 1957. Melting relations of the common rock-forming oxides. J. Am. Ceram. Soc. 40, 215–235.
Seggiani, M., 1999. Empirical correlations of the ash fusion temperatures and temperature of critical viscosity for coal and biomass ashes. Fuel 78, 1121–1125.
Shacklette, H.T., Boerngen, J.G., 1984. Element Concentrations in Soils and Other Surficial Materials of the Conterminous United States. U.S. Geological Survey Professional Paper 1270. United States Government Printing Office, Washington, D.C.
Shelby, J.E., 2005. Introduction to Glass Science and Technology. Cambridge University Press.
Stevanovic, M., 1997. The age of clay: the social dynamics of house destruction. J. Anthropol. Archaeol. 16, 334–395.
Stordeur, D., Abbes, F., 2002. Du PPNA au PPNB: mise en lumière d'une phase de transition à Jerf el Ahmar (Syrie). Bull. Société Préhistorique Française 99, 563–595.
Stracher, G.B. (Ed.), 2007. Geology of Coal Fires: Case Studies from Around the World. Reviews in Engineering Geology, vol. 18. Geological Society of America, 283 pp.
Surovell, T.A., Holliday, V.T., Gingerich, J.A.M., Ketron, C., Haynes Jr., C.V., Hilman, I., Wagner, D.P., Johnsond, E., Claeys, P., 2009. An independent evaluation of the Younger Dryas extraterrestrial impact hypothesis. Proc. Natl. Acad. Sci. 106, 18155–18158.
Thornber, C.R., Sherrod, D.R., Siems, D.F., Heliker, C.C., Meeker, G.P., Oscarson, R.L., Kauahikaua, J.P., 2002. Whole-rock and Glass Major-element Geochemistry of Kilauea Volcano, Hawaii, Near-vent Eruptive Products: September 1994 through September 2001. Open File Report 02–17. U.S. Geological Survey.
Thy, P., Segobye, A.K., Ming, D.W., 1995. Implications of Prehistoric glassy biomass slag from East-Central Botswana. J. Archaeol. Sci. 22, 629–637.
Thy, P., Yu, C., Jenkins, B.M., Lesher, C.E., 2013a. Inorganic composition and environmental impact of biomass. Energy Fuels 27, 39–69.
Thy, P., Yu, C., Blunk, S.L., Jenkins, B.M., 2013b. Inorganic composition of saline-irrigated biomass. Water Air Soil Pollut. 224, 1617–1634.
Tringham, R., 2005. Weaving house life and death into places: a blueprint for a hypermedia narrative. In: Bailey, D., Whittle, A., Cummings, V. (Eds.), (Un) settling the Neolithic. Oxbow Books, Oxford, UK, pp. 98–111.
Turekian, K.K., Wedepohl, K.H., 1961. Distribution of the elements in some major units of the Earth's crust. Geological Soc. Am. Bull. 72, 175–192.
Tyler, G., 2004. Rare earth elements in soil and plant systems – a review. Plant Soil 267, 191–206.
van Hoesel, A., Hoek, W.Z., Pennock, G.M., Drury, M.R., 2014. They Younger Dryas impact hypothesis: a critical review. Quat. Sci. Rev. 83, 95–114.

Vapnik, Y., Sharygin, V.V., Sokol, E.A., Shagam, R., 2007. Paralavas in a combustion metamorphic complex: Hatrurim Basin, Israel. In: Stracher, G.B. (Ed.), Geology of Coal Fires: Case Studies from Around the World. Reviews in Engineering Geology, vol. 18. Geological Society of America, Washington DC, pp. 133–153.

Vassilev, S.V., Menendez, R., Diaz-Somoano, M., Martinez-Tarazona, M.R., 2004. Phase-mineral and chemical composition of coal fly ashes as a basis for their multicomponent utilization. 2. Characterization of ceramic cenosphere and salt concentrates. Fuel 83, 585–603.

Veizer, J., 1983. Trace elements and isotopes in sedimentary carbonates. In: Reeder, R.J. (Ed.), Carbonate: Mineralogy and Chemistry. Reviews in Mineralogy, vol. 11. American Mineralogical Society, Washington DC, pp. 265–299.

Venkatasubbaiah, P.C., 2012. A Preliminary study on the Ashmound sites in the Lower Tungabhadra region of Andhra Pradesh. Anc. Asia 3, 36–48.

Volovetsky, M.V., Rusakov, V.S., Lukanin, O.A., Kargaltsev, A.A., 2010. Study of oxygen fugacity influence on redox state of iron in granitoidic melts. J. Phys. Conf. Ser. 217, 1–4.

Willcox, G., 2011. Témoignages d'une agriculture précoce à Shillourokambos. étude du Secteur 1. In: Guilaine, Jean, Briois, François, Vigne, Jean-Denis (Eds.), Shillourokambos, un établissement néolithique pré-céramique à Chypre les fouilles du secteur 1. Errance, Paris, pp. 569–575.

Willcox, G., Fornite, S., 1999. Impressions of wild cereal chaff in pisé from the tenth millennium at Jerf el Ahmar and Mureybet: northern Syria. Veg. Hist. Archaeobot. 8 (1–2), 14–21.

Willcox, G., Stordeur, D., 2012. Large-scale cereal processing before domestication during the tenth millennium BC cal. in northern Syria. Antiquity 86 (331), 99–114.

Willcox, G., Herveux, L., 2013. Late Pleistocene/early Holocene charred plant remains: preliminary report. In: Mazurowski, R.F., Kanjou, Y. (Eds.), Tell Qaramel 1999–2007. Protoneolithic and Early Pre-pottery Neolithic Settlement in Northern Syria. PCMA, Warsaw, 120/130.

Willcox, G., Fornite, S., Herveux, L., 2008. Early Holocene cultivation before domestication in northern Syria. Veg. Hist. Archaeobot. 17, 313–325.

Wittke, J.H., Weaver, J.C., Bunch, T.E., Kennett, J.P., Kennett, D.J., Moore, A.M.T., Hillman, G.C., Tankersley, K.B., Goodyear, A.C., Moore, C.R., Daniel Jr., I.R., Ray, J.H., Lopinot, N.H., Ferraro, D., Israde-Alcántara, I., Bischoff, J.L., DeCarli, P.S., Hermes, R.E., Kloosterman, J.B., Revay, Z., Howard, G.A., Kimbel, D.R., Kletetschka, G., Nabelek, L., Lipo, C.P., Sakai, S., West, A., Firestone, R.B., 2013. Evidence for deposition of 10 million tonnes of impact spherules across four continents 12,800 y ago. Natl. Acad. Sci. 110, E2088–E2097.

Wu, Y., Sharma, M., LeCompte, M.A., Demitroff, M.N., Landis, J.D., 2013. Origin and provenance of spherules and magnetic grains at the Younger Dryan boundary. Proc. Natl. Acad. Sci. 110, E3557–E3566.

Youngblood, E., Fredriksson, B.J., Kraut, F., Fredriksson, K., 1978. Celtic vitrified forts: implications of a chemical-petrological study of glasses and source rocks. J. Archaeol. Sci. 5, 99–121.

Zeuner, F.E., 1959. On the origin of the cinder mounds of the Bellary District, India. Bull. Inst. Archaeol. 2, 37–44.